

Supporting Information

© Wiley-VCH 2015

69451 Weinheim, Germany

**Random-Graft Polymer-Directed Synthesis of Inorganic
Mesostructures with Ultrathin Frameworks****

*Changbum Jo, Yongbeom Seo, Kanghee Cho, Jaeheon Kim, Hye Sun Shin, Munhee Lee, Jeong-Chul Kim, Sang Ouk Kim, Jeong Yong Lee, Hyotcherl Ihee, and Ryong Ryoo**

anie_201310748_sm_miscellaneous_information.pdf

Supporting Information

Section S1. MFI zeolite nanosponge

1.1. Synthesis details for MFI zeolite nanosponge

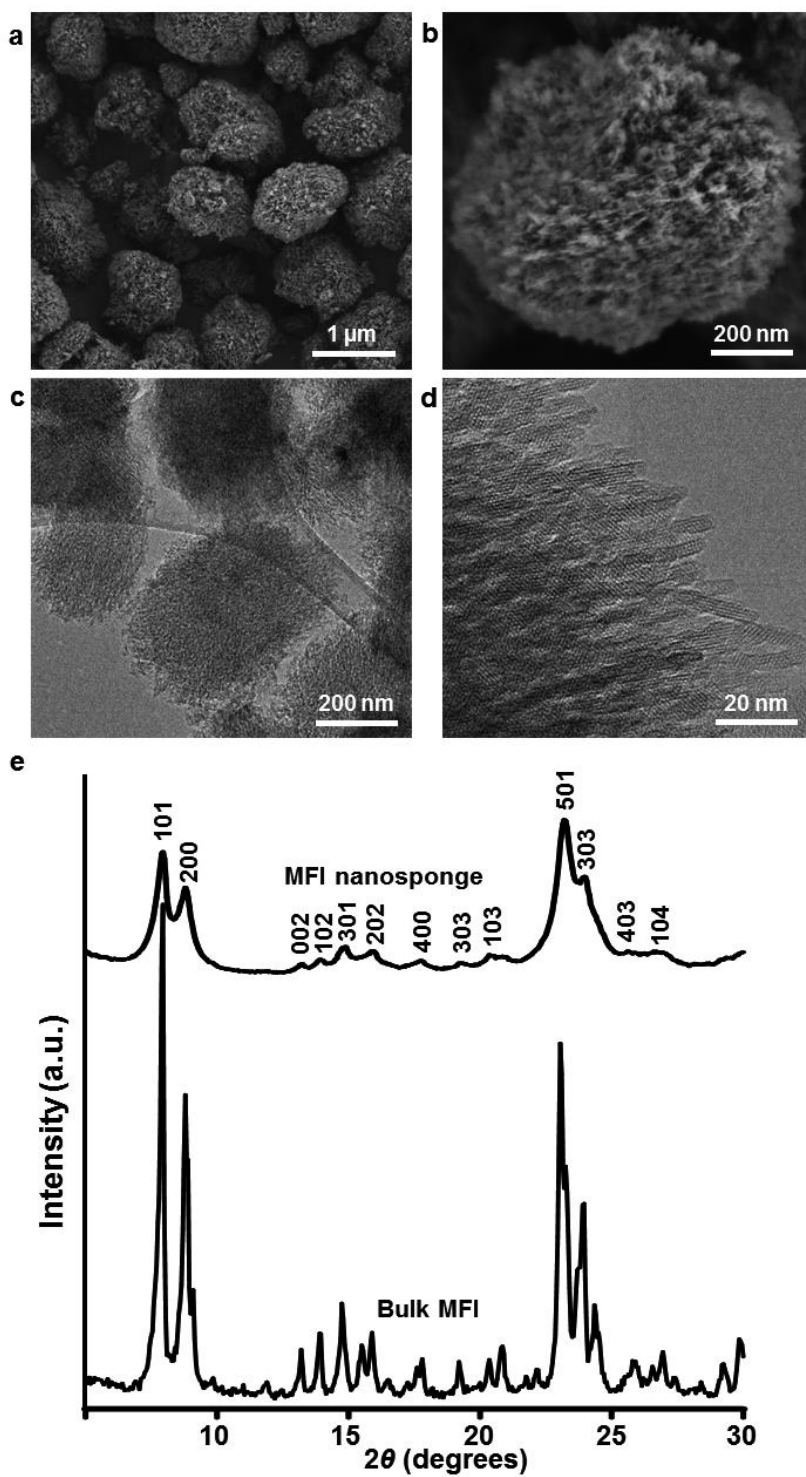
A series of random copolymers, poly[(styrene)-*co*-(4-chloromethylstyrene)], with different ratios of 4-chloromethylstyrene (4-CMS, TCI, 90%) were synthesized via nitroxide-mediated radical polymerization according to the previous report (*Bull. Korean Chem. Soc.* **23**, 1833). 4-CMS and styrene were used as monomers. The percentage of 4-CMS in the total monomer was 10, 20, 40, 60 or 80%. A typical synthesis of a poly[(styrene)-*co*-(4-chloromethylstyrene)] was as follows: 0.0342 g of (2,2,6,6-Tetramethylpiperidin-1-yl)oxyl (TEMPO, Aldrich) and 0.018 g of α, α' -azobis(isobutyronitrile) (Junsei, 98%) were dissolved in 13 ml of chlorobenzene (Aldrich, 99%). A mixture of 4-CMS and styrene (sum of moles of 4-CMS and styrene: 35 mmol) was added to the chlorobenzene solution containing radical initiators. The mixture was degassed in a Schlenk flask by two cycles of freeze-vacuum-thaw using a liquid nitrogen trap. The Schlenk flask was moved to an oil bath and heated for 2 d at 393 K with stirring. After cooling to room temperature, the poly[(styrene)-*co*-(4-chloromethylstyrene)] was precipitated with methanol, filtered and dried in a vacuum oven at 303 K for 12 h. The molecular weight (M_w) and polydispersity index of the resultant polymers were 100,000/3.6 (80mol% of 4-CMS), 81,000/2.1 (60% of 4-CMS), 75,000/2.3 (40% of 4-CMS), 27000/2.0 (20% of 4-CMS), and 26000/2.1 (10% of 4-CMS), respectively.

For the synthesis of $[\text{C}_6\text{H}_{13}\text{-N}^+(\text{CH}_3)_2\text{-C}_6\text{H}_{12}\text{-N}^+(\text{CH}_3)_2\text{-C}_6\text{H}_{12}\text{-N}(\text{CH}_3)_2][\text{Br}^-]_2$, 10 mmol of $[\text{C}_6\text{H}_{13}\text{-N}^+(\text{CH}_3)_2\text{-C}_6\text{H}_{12}\text{-Br}][\text{Br}^-]$ (*Chem. Mater.* **23**, 5131 for synthesis details) and 100 mmol of *N,N,N',N'*-tetramethyl-1,6-diaminohexane were dissolved in 200 ml of ethanol and heated at 323 K with magnetic stirring. After the reaction was finished, the product was obtained by filtration.

Poly[(styrene)-*co*-(4-chloromethylstyrene)] was reacted with $[\text{C}_6\text{H}_{13}\text{-N}^+(\text{CH}_3)_2\text{-C}_6\text{H}_{12}\text{-N}^+(\text{CH}_3)_2\text{-C}_6\text{H}_{12}\text{-N}(\text{CH}_3)_2][\text{Br}^-]_2$ in dimethylformamide (DMF, Junsei, 99.5%) at 313 K. The stoichiometric ratio of the chloromethyl groups to $[\text{C}_6\text{H}_{13}\text{-N}^+(\text{CH}_3)_2\text{-C}_6\text{H}_{12}\text{-N}^+(\text{CH}_3)_2\text{-C}_6\text{H}_{12}\text{-N}(\text{CH}_3)_2][\text{Br}^-]_2$ was 1:1. The resulting polymers are functionalized with $-\text{N}^+(\text{CH}_3)_2\text{-C}_6\text{H}_{12}\text{-N}^+(\text{CH}_3)_2\text{-C}_6\text{H}_{12}\text{-N}^+(\text{CH}_3)_2\text{-C}_6\text{H}_{13}$. This moiety is denoted by 'N₃-SDA'. The product was confirmed by ¹H NMR.

MFI zeolites were hydrothermally synthesized using N₃-SDA functionalized polymers as the zeolite SDAs. Sodium silicate (26.5% SiO₂, 10.6% Na₂O, Aldrich), Al₂SO₄·18H₂O (98%, Aldrich), H₂SO₄ (47%, Wako), and the polymer were added at once into a polypropylene bottle. The molar composition of the synthesis gel was 100 SiO₂: 1 Al₂O₃: 39 Na₂O: 27 H₂SO₄: 400 ethanol: *p* SDA-equipped polymer: 6000 H₂O, where *p* was varied from 0.1 to 0.7 to adjust the ratio of SiO₂/N⁺ to 2.5. The bottle was immediately shaken vigorously by hand. After further mixing by a magnetic stirrer for 6 h in an oven at 333 K, the resultant gel was transferred into a Teflon-lined stainless steel autoclave. The autoclave was tumbled with mixing baffles in an oven for 6.5d at 423 K. The precipitated product was filtered, washed with distilled water and, finally dried in a convection oven at 373 K. For measurement of pore size distribution, the samples were calcined at 853 K for 4 h in flowing air. No zeolite crystals were obtained under the same conditions without polymers, confirming that the amorphous polymer functioned as MFI zeolite SDAs.

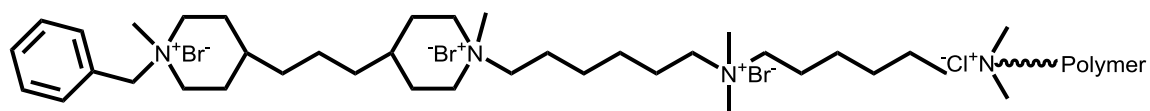
1.2. Characterization results of MFI zeolite nanosponge synthesized using linear polystyrene functionalized with N₃-SDA groups: (a) and (b) SEM images, (c) and (d) TEM images, (e) wide-angle XRD patterns.



Section S2. Beta zeolite nanosponge and ATO-type AlPO_4 nanosponge synthesized using polymer-directed crystallization mechanism

2.1. Preparation of zeolite beta nanosponge

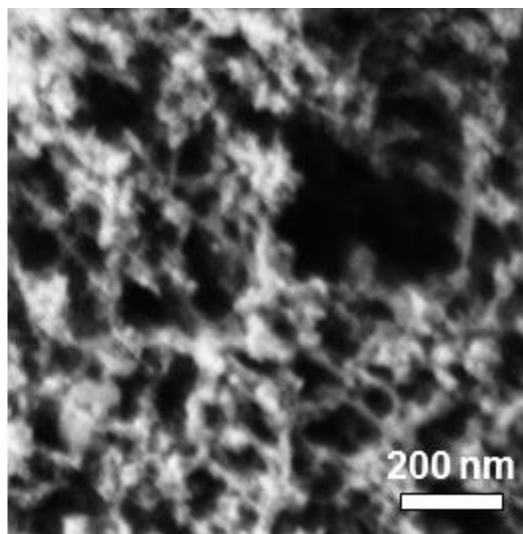
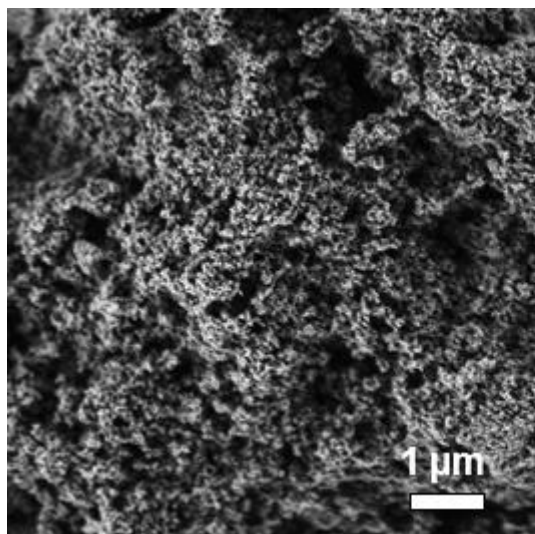
A beta zeolite nanosponge was hydrothermally synthesized using linear polystyrene functionalized with tetra-ammonium containing two piperidinium groups. The functionalized tetra-ammonium group is denoted by 'Piper₂N₂' and its molecular structure is shown after this paragraph. The N₄-SDA functionalized polymer, fumed silica (Aldrich), sodium aluminate (40-45% Na₂O, 50-56% Al₂O₃, Aldrich), and NaOH were mixed with distilled water to obtain a gel composition of 30 SiO₂: 1 Al₂O₃: 0.03 polymer: 6.67 Na₂O: 3000 H₂O. The mixed gel was stirred at 333 K for 12 h and transferred to a Teflon-coated stainless-steel autoclave. The autoclave was heated at 413 K for 5 d while tumbling. The precipitated product was filtered, washed with distilled water, and finally, dried in a convection oven at 373 K. A sample for pore-size analysis was calcined at 823 K for 4 h under flowing air, in order to remove the organic polymer.



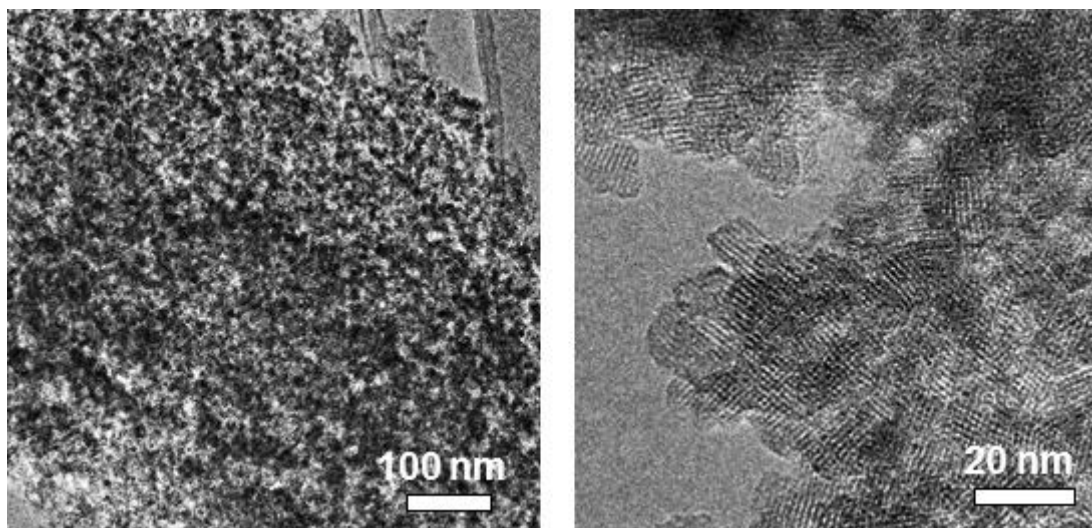
< N₄-SDA for beta zeolite synthesis >

2.2. Characterization results of zeolite beta nanosponge synthesized using linear polystyrene functionalized with Piper₂N₂.

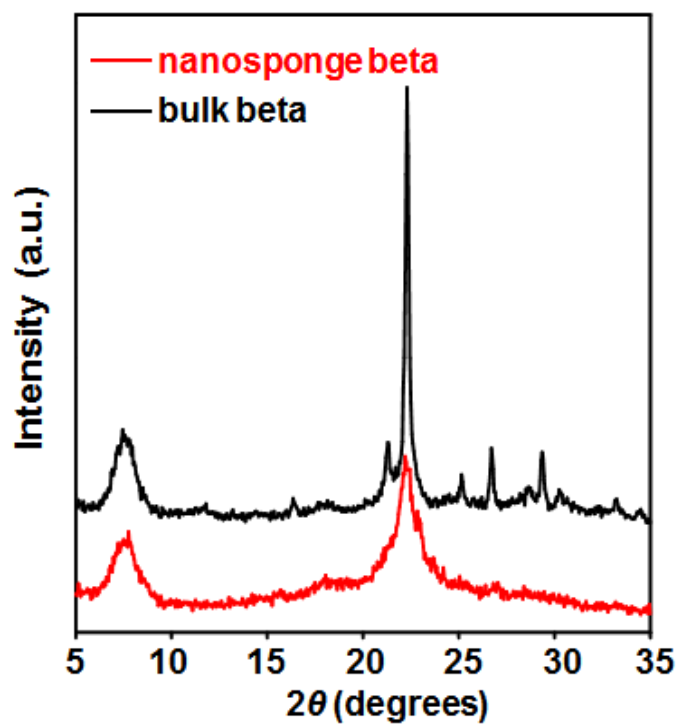
(a) SEM images of zeolite beta nanosponge.



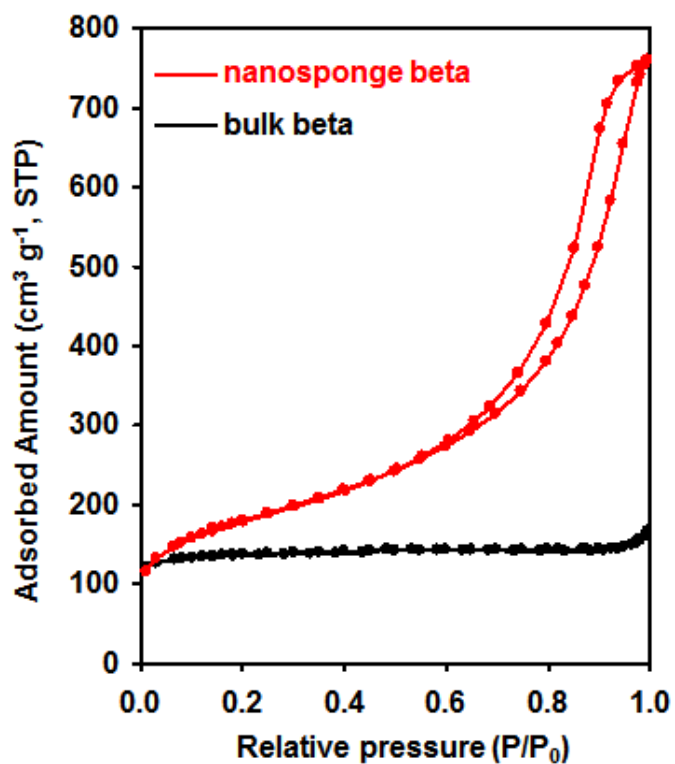
(b) TEM images of zeolite beta nanosponge.



(c) XRD patterns of the zeolite beta nanosponge (red) and bulk beta (black).



(d) N₂ isotherms of zeolite beta nanosponge (red) and bulk beta (black). The specific BET surface areas of the beta nanosponge and bulk beta measured by the BET method were 790 and 550 m² g⁻¹, respectively.

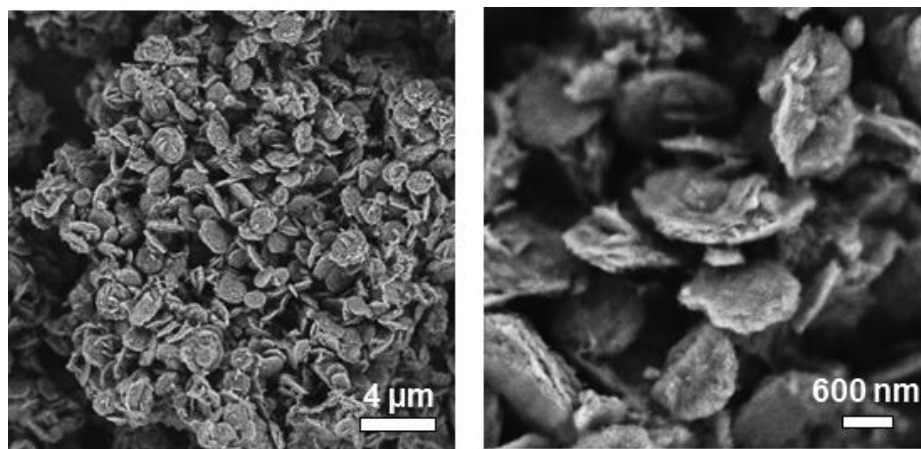


2.3. Preparation of ATO-type AlPO_4 nanosponge

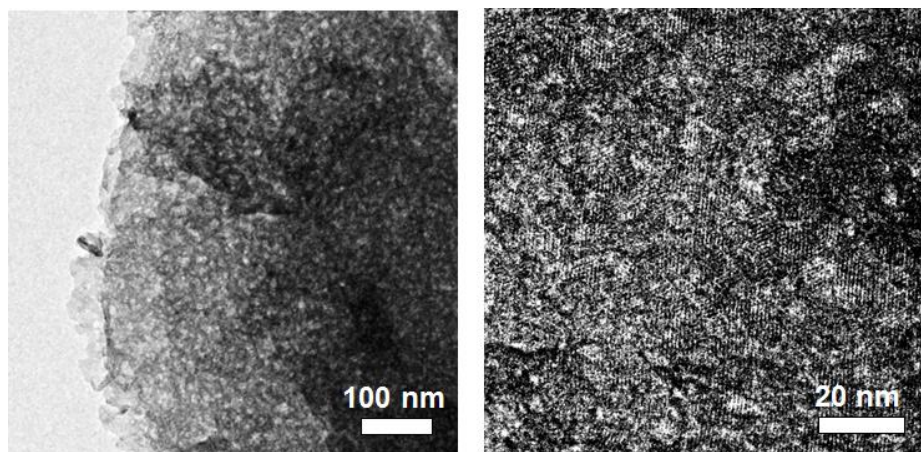
A crystalline AlPO_4 nanosponge was hydrothermally synthesized using the same polymer (polystyrene functionalized with N_3 -SDA) used in the synthesis of the MFI nanosponge. An aqueous solution of halide-form polymer was passed through a column packed with anion exchange resin (MTO-Dowex SBR LCNG OH form, Supelco) for conversion to the hydroxide form. In a typical synthesis experiment, pseudoboehmite (Capatal Alumina, 75 wt%), H_3PO_4 (Sigma-Aldrich, 85 wt%), and distilled water were mixed vigorously for 8 h. The hydroxide form of the polymer was added to the AlPO_4 precursor solution and the resultant reaction gel was stirred for 2 h. The molar composition of the resultant gel was 1.0 Al_2O_3 : 1.0 P_2O_5 : 500 H_2O : 0.005 polymer. The mixture was heated in an oven at 453 K with tumbling. The precipitate solids were collected by filtration at 1 d of hydrothermal synthesis, washed with distilled water, and finally dried in a convection oven at 373 K. The sample for pore-size analysis was calcined under air flow at 823 K.

2.4. Characterization results of ATO-type AlPO_4 nanosponge synthesized using linear polystyrene functionalized with N_3 -SDA.

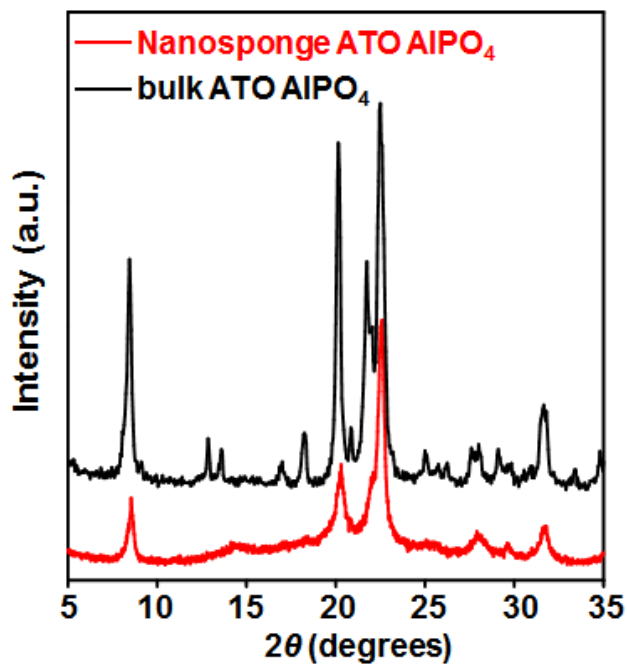
(a) SEM images of ATO-type AlPO_4 nanosponge.



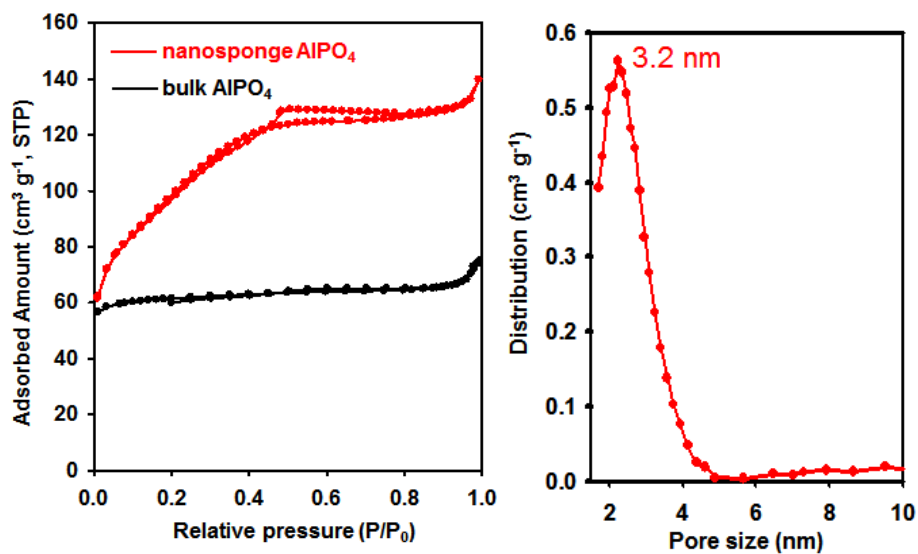
(b) TEM images of ATO-type AlPO_4 nanosponge.



(c) XRD patterns of ATO-type AlPO_4 nanosponge (red) and bulk ATO-type AlPO_4 (black).

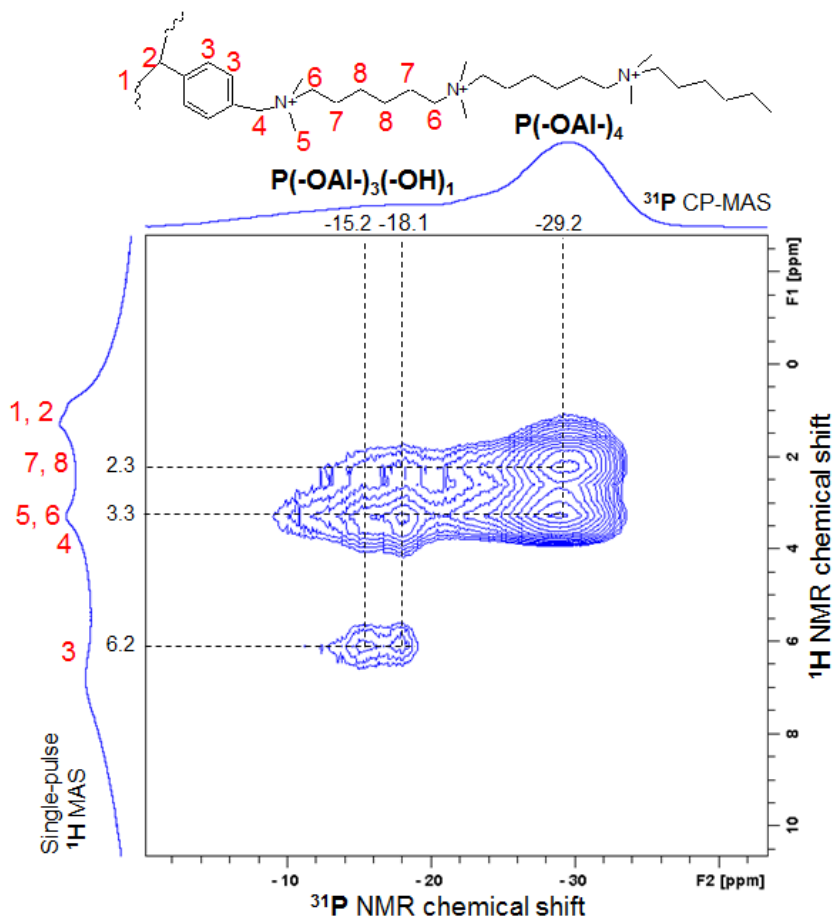


(d) N_2 isotherms and mesopore size distribution of ATO-type AlPO_4 nanosponge (red) and bulk ATO-type AlPO_4 (black). The specific BET surface areas of the AlPO_4 nanosponge and bulk AlPO_4 measured by the BET method were 350 and 100 m^2 g^{-1} , respectively.



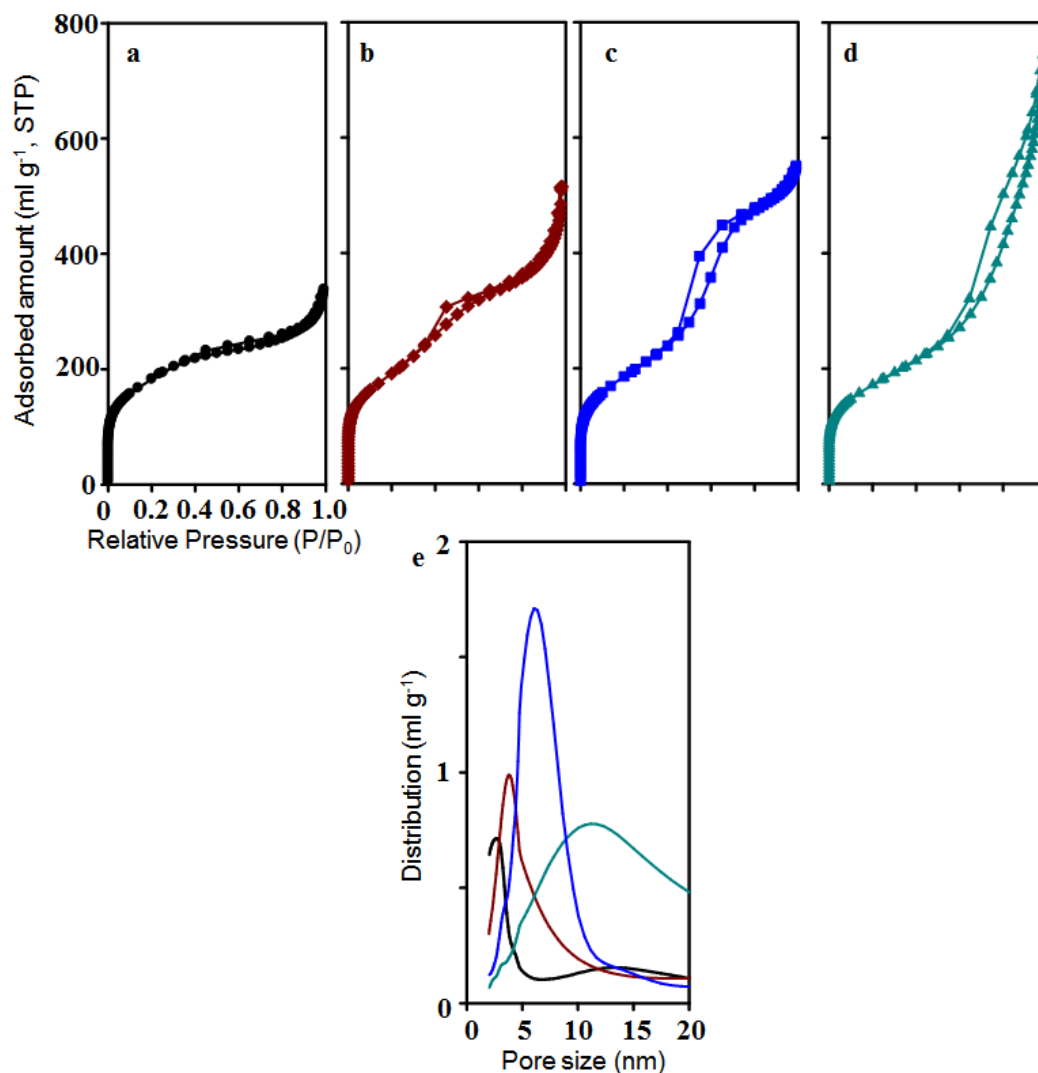
Section S3. Solid-state two-dimensional $^{31}\text{P}\{^1\text{H}\}$ HETCOR NMR spectrum of polymer- AlPO_4 mesostructure

One-dimensional ^{31}P CP-MAS and single-pulse ^1H MAS spectra are shown along the horizontal and vertical axes, respectively. A schematic diagram of the N_3 -SDA grafted polymer is labelled with ^1H signal assignments of covalently bonded protons. The two-dimensional $^{31}\text{P}\{^1\text{H}\}$ HETCOR NMR spectrum shows the strong interaction between the polymer species and the AlPO_4 framework. The strong two-dimensional correlated signal intensities associated with $[\text{P}(\text{-OAl-})_4, -29.2 \text{ ppm}]$ and $[\text{P}(\text{-OAl-})_3(\text{-OH})_1, -15 \sim -18 \text{ ppm}]$ ^{31}P framework species and $-\text{N}^+\text{CH}_3$, $-\text{N}^+\text{CH}_2-$ (alpha proton) and $-\text{N}^+\text{CH}_2\text{CH}_2-$ (beta proton) ^1H moieties at 3.4 and 2.3 ppm provide direct evidence for intermolecular interactions between N_3 -SDA and the AlPO_4 framework. On the other hand, the ^1H signal at 6.2 ppm associated with the $-\text{C}_6\text{H}_5-$ styrenic backbone shows only a weak 2D correlated signal with the $\text{P}(\text{-OAl-})_3(\text{-OH})_1$. Thus, the N_3 -SDA of polymer backbones were certainly embedded in the microporous framework of AlPO_4 .



Section S4. N₂ isotherms and their corresponding mesopore size distributions of a series of MFI zeolite nanosponges.

MFI zeolite nanosponges were synthesized using a series of the polymer with different degrees of N₃-SDA functionalization along the polymer chains. Depending on the degree of N₃-SDA functionalization, the zeolite nanosponge samples are denoted by 'ZS-N₃(c)', where 'c' means the ratio of SDA-equipped styrenic units in total of the styrenic units. N₂ isotherms (a-d) of 'ZS-N₃(0.8)' (black), 'ZS-N₃(0.6)' (brown), 'ZS-N₃(0.4)' (blue), and 'ZS-N₃(0.2)' (dark-cyan) are shown. Mesopore size distributions of the MFI zeolite nanosponges (e) were calculated by the non-local density functional theory, and smoothed using FFT filtering methods with a window of five points. This figure shows that the mode diameter gradually increases from 2.7 to 11.2 nm as the degree of N₃-SDA functionalization decreases from 80% to 20% styrene unit. This can be explained by the increase of fringing polymer portion compared to the zeolite crystal domain. Below 10% functionalization, however, no zeolite was formed.



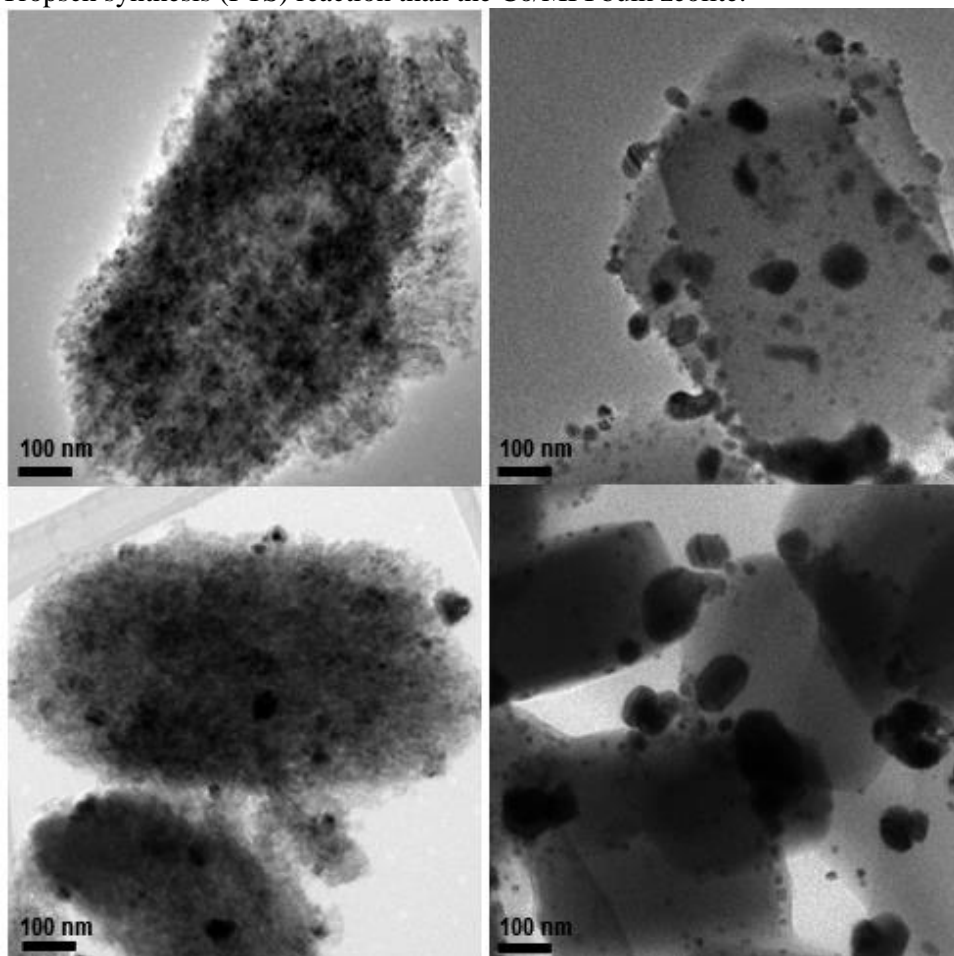
Section S5. Fischer-Tropsch synthesis over Co/MFI zeolites

5.1. Synthesis of Co/MFI zeolites

Before cobalt loading on MFI zeolites, all the MFI zeolites were first NH_4^+ -ion exchanged three times with a 1 M NH_4NO_3 solution ($\text{NH}_4\text{NO}_3/\text{Al} = 10$), and then subsequently converted to the H^+ form through calcination in air at 823 K. The cobalt species was introduced into the MFI zeolites by the aqueous incipient wetness impregnation method using the aqueous solution of cobalt nitrate ($\text{Co}(\text{NO}_3)_2 \cdot 6\text{H}_2\text{O}$, Fluka). In a typical preparation, 0.273 g of the cobalt precursor was impregnated in 0.5 g of the MFI zeolite to obtain 10 wt% Co content in the final catalysts. The Co-supported MFI zeolite samples were dried in a convection oven at 373 K for 12 h and calcined by O_2 (99.9%, flow rate = $400 \text{ cm}^3 \text{ min}^{-1}$) at 573 K for 4 h.

5.2. TEM images of (left column) Co/MFI zeolite nanosponge and (right column) Co/MFI bulk zeolite; (top) as-prepared and (bottom) after 50 h of FTS reaction

-The Co/MFI zeolite nanosponge exhibited much higher resistance to the metal agglomeration during the Fischer-Tropsch synthesis (FTS) reaction than the Co/MFI bulk zeolite.

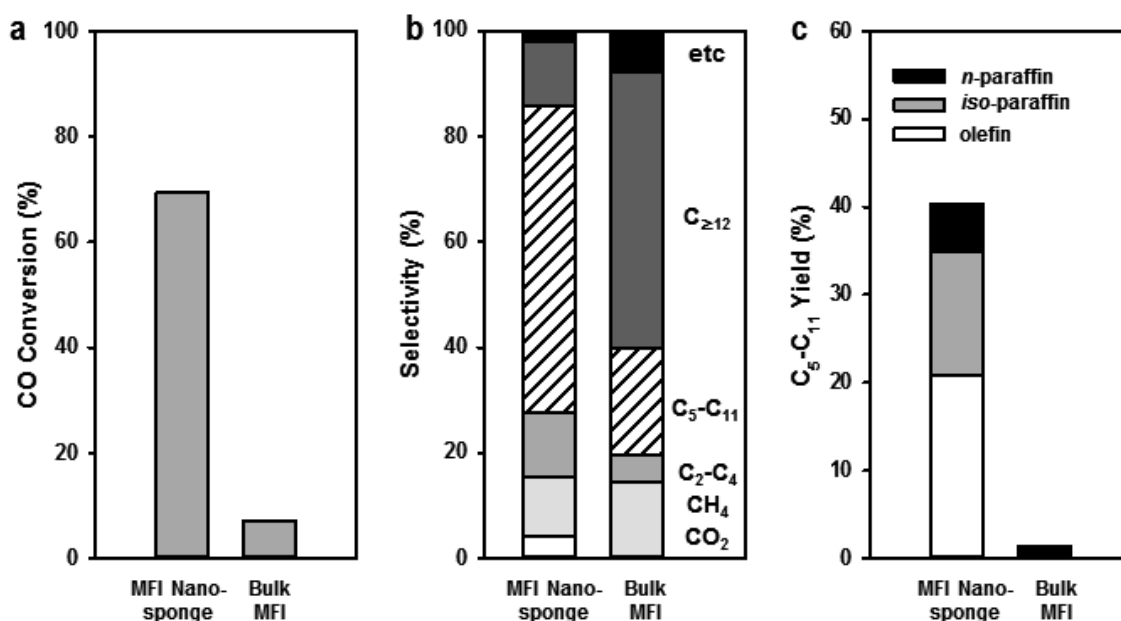


5.3. FTS reaction measurement

FTS was conducted in a stainless steel fixed-bed reactor (7 mm inner diameter) using 0.5 g of Co/MFI zeolite catalysts. Prior to the FTS reaction test, the catalyst was activated by high-purity H₂ (99.999%, flow rate = 50 cm³ min⁻¹) at 673 K for 12 h. The temperature decreased to room temperature. The H₂ flow was changed to syngas (H₂/CO volume ratio of 2) with a flow rate of 20 cm³ min⁻¹, and the syngas pressure in the reactor was increased to 20 bar. Argon was added to the syngas with 10 mol% concentration, as an internal standard for the calculation of CO conversion. FTS reaction was performed at 493 K. The gas-phase products were analyzed using an online gas chromatograph (Younglin, Acme-6000) equipped with a flame ionization detector and a thermal conductivity detector. The products were separated by Gaspro (Agilent) and Porapak Q (Supelco) columns. Liquid-phase products were collected in a cold trap (278 K) and analyzed off-line with a gas chromatograph equipped with an HP-1 column (Agilent). The CO conversion and product selectivity were determined at 50 h of reaction time. Selectivity was reported as the percentage of CO converted into a certain product expressed in C atoms.

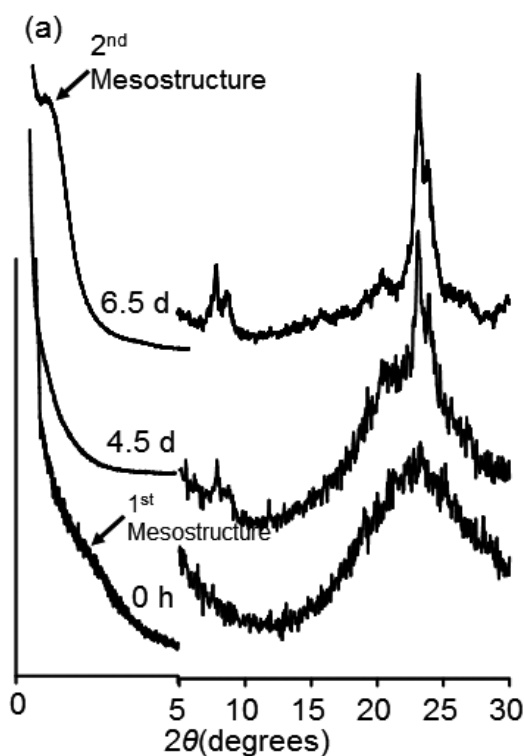
5.4. Catalytic performance of Co/MFI nanosponge and Co/MFI bulk zeolite in FTS

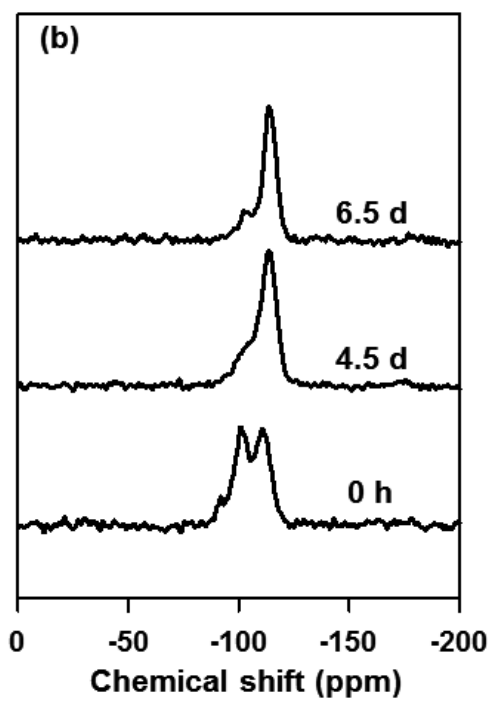
Reaction conditions were as follows: weight of catalyst = 0.5 g, gas hourly space velocity = 2.4 L h⁻¹ g⁻¹, reaction temperature = 493 K, H₂/CO in reactant syngas = 2, pressure of the syngas = 20 bar. (a) CO conversion at 50 h of the reaction time, (b) product selectivity according to the number of carbon atoms in the molecules, (c) product yield (CO conversion * product selectivity) of olefin, isomer paraffin, and normal paraffin in the range from C₅ to C₁₁. The MFI zeolite nanosponge displayed much better catalytic performance (high conversion of CO, high selectivity to branched hydrocarbons in the gasoline range) than bulk MFI zeolite.



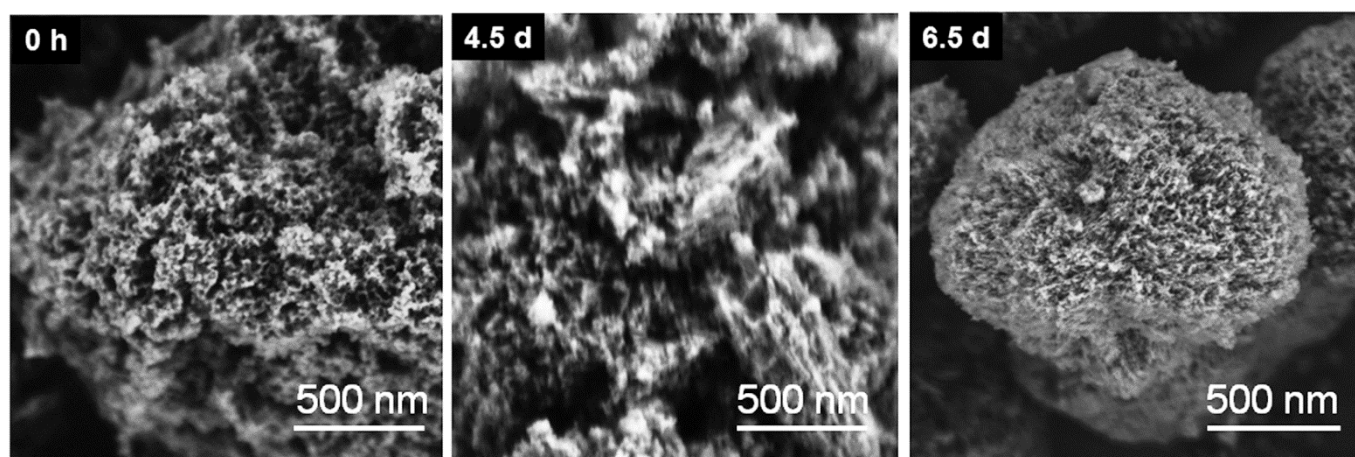
Section S6. Structure analysis of MFI zeolite nanosponges along the time line of the zeolite synthesis process using XRD, solid state ^{29}Si NMR, SEM, and TEM.

Hydrothermal synthesis of MFI zeolite nanosponge was performed with a random copolymer functionalized with $\text{N}_3\text{-SDA}$ as the zeolite SDA. During the hydrothermal treatment, solid precipitates were collected by filtration at 0 h, 4.5 d, and 6.5 d of hydrothermal reaction time. The solid precipitates were analyzed with (a) XRD, (b) solid-state ^{29}Si NMR, (c) TEM, and (d) SEM. In the case of 0 h sample, TEM image shows that the precipitate was composed of mesostructured polymer-inorganic composite. Small angle XRD pattern of this sample shows good agreement with TEM image, indicating the short-range ordering of mesostructure. The mesopore wall of this sample is amorphous silica. It was confirmed by XRD analysis. Solid-state ^{29}Si NMR showed that a large amount of Q^2 (90 ppm) and Q^3 (100 ppm) Si species, indicating that the frameworks are amorphous framework. The results of the structure investigation for 0 h sample indicated that the silica framework formed initially the mesostructure with the polymer, immediately after mixing silicate precursor and the polymer. The mesostructured amorphous gel was then transformed to a crystalline framework upon the subsequent hydrothermal treatment. After 4.5d of hydrothermal reaction, the XRD peaks corresponding to MFI zeolites could be observed in XRD pattern. However, broad reflection peak is still observed in the range of $15 \sim 25^\circ$ of 2θ , which corresponds to amorphous silica. This result indicated that the mesoporous wall still contained amorphous phase. In NMR spectra of 4.5 d sample, the intensities of Q^2 and Q^3 peaks are very small, as compared to that of 0 h sample. This result shows good agreement with the result of XRD analysis. During the transformation of the mesoporous silica wall, the silica framework still retained the mesostructure, although the framework thickness and inter-layer spacing of the mesostructure increased. Zeolites were fully crystallized after 6.5 d of hydrothermal reaction, which could be confirmed by XRD and solid-state ^{29}Si NMR spectroscopy. At this final stage, a well resolved Bragg reflection peak centered at $2\theta = 0.83^\circ$ was observed in XRD pattern. This reflection peak indicated that there should be significant short-range structural ordering in the zeolite nanosponge. For a disordered mesostructure, this kind of structure coherence only occurs when uniform mesopores are retained between zeolite frameworks of uniform thickness. Since the reflection peak centered at $2\theta = 0.8^\circ$ was never observed at initial stage (*i.e.* 0 h), the zeolite crystallization could induce the short-range structural ordering in the final product (*i.e.* 6.5 d). This mechanistic study strongly supported our mechanism proposed in the present paper.

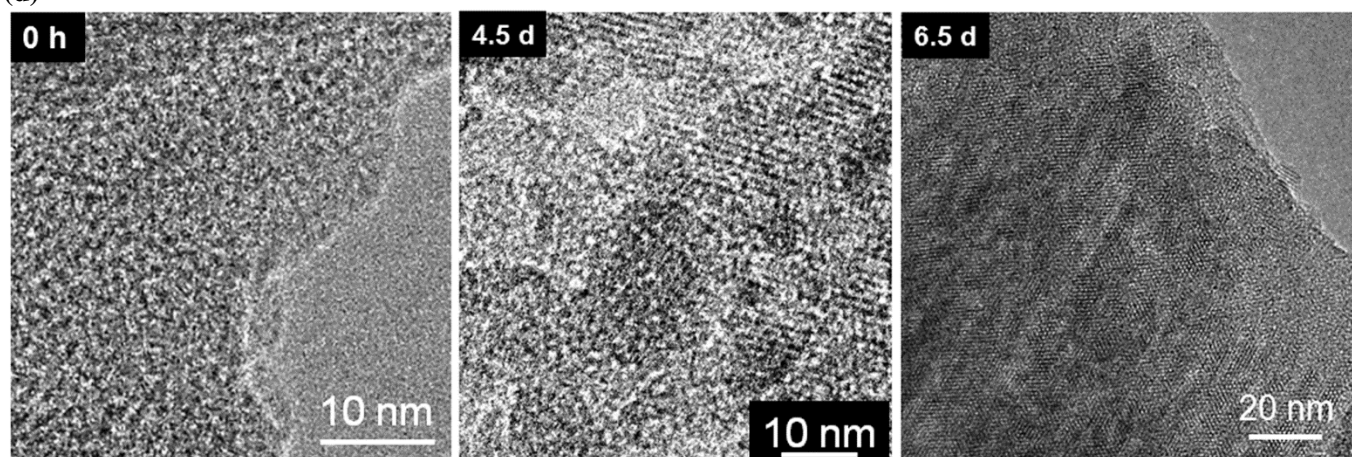




(c)



(d)



Section S7. Mesostructured titania synthesized using a polymer-directed crystallization mechanism

7.1. Preparation of mesostructured titania

(a) Procedure A

Mesostructured titania was solvothermally synthesized using polyacrylic acid (PAA, Sigma-Aldrich, M_n : 450,000) in dimethylformamide (DMF, Sigma-Aldrich, 99.8%). In a typical synthesis, titanium isopropoxide (Sigma-Aldrich, 97%) was dissolved in DMF with magnetic stirring. Degassed PAA was dissolved in DMF with magnetic stirring. The PAA solution was quickly added to the titanium isopropoxide solution and stirred at room temperature for 2 h. Subsequently, distilled water was added. The molar composition of the synthesis gel was 1 TiO₂: p [-CH(COOH)CH₂-]: 20 H₂O: 600 DMF, where ' p ' is 0.33 for nanosponge and 2 for nanosheet. The mixture was transferred into a Teflon-lined autoclave and then heated in an oven at 373 K. The product was collected by centrifugation and dried in a convection oven at 373 K. The mesopores can be opened by calcination treatment in air at 623 K, which decomposes the polymer. A trace amount of remaining carbonaceous residue in the samples could be completely removed with ozone flow at 573 K.

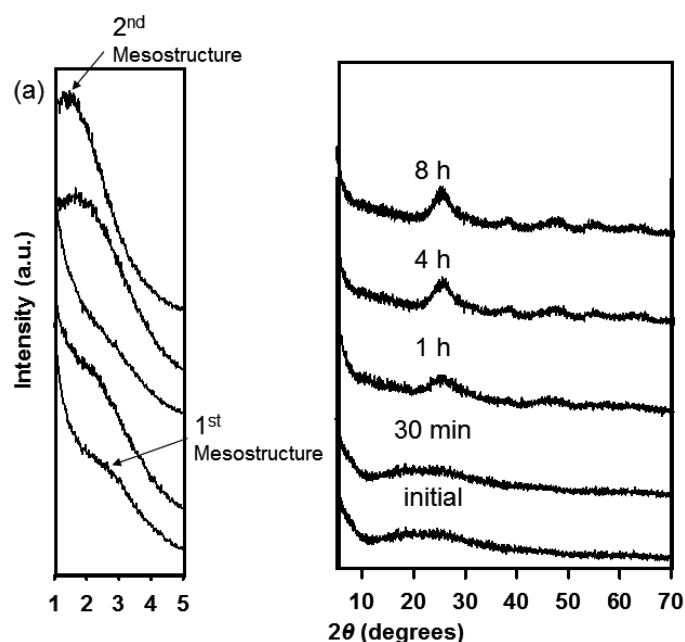
(b) Procedure B

Titania nanosheet was solvothermally synthesized using poly(4-vinylphenol-*co*-methyl methacrylate) (PVP-*co*-PMMA, Sigma-Aldrich) in DMF solution. In a typical synthesis, 0.72g of PVP-*co*-PMMA was dissolved in 25 ml of DMF with magnetic stirring. 0.67 ml of titanium chloride (Sigma-Aldrich, 99.9%) was added to this solution dropwise with the stirring. The solution was refluxed for 1 d to form phenol-Ti-O bonding, completely (*J. Mol. Catal. A.*, **2012**, 355, 161). 0.33 ml of distilled water was added to this solution dropwise, and subsequently, 3.4 ml of distilled triethylamine was added for neutralizing the solution. The mixture was transferred to a Teflon-lined autoclave and then heated in an oven at 423 K for 3 d. The product was collected by centrifugation and dried in a convection oven at 373 K. The mesopores can be opened by calcination treatment in air at 623 K, which decomposes the polymer. A trace amount of remaining carbonaceous residue in the samples could be completely removed with ozone flow at 573 K.

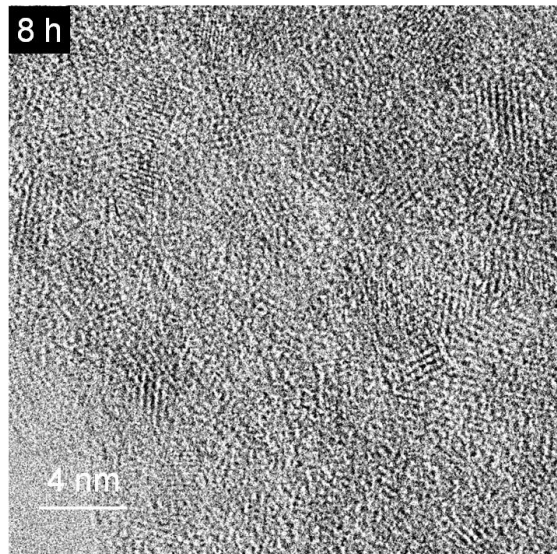
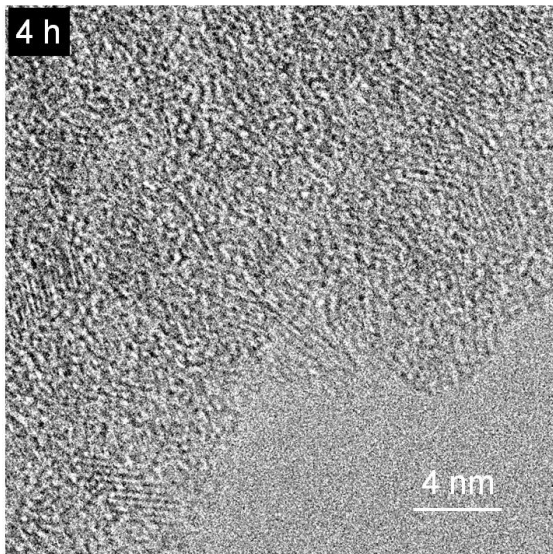
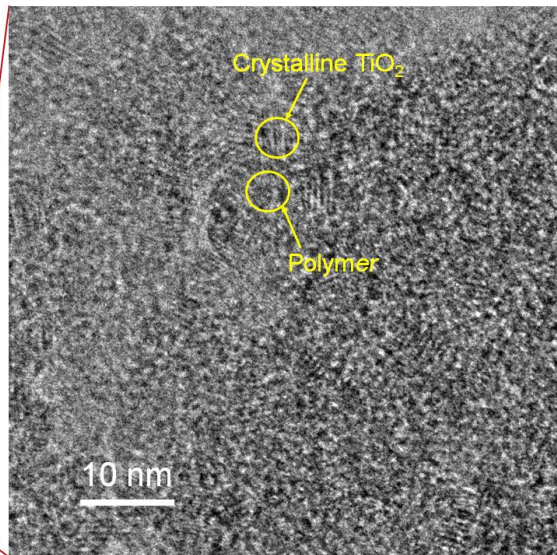
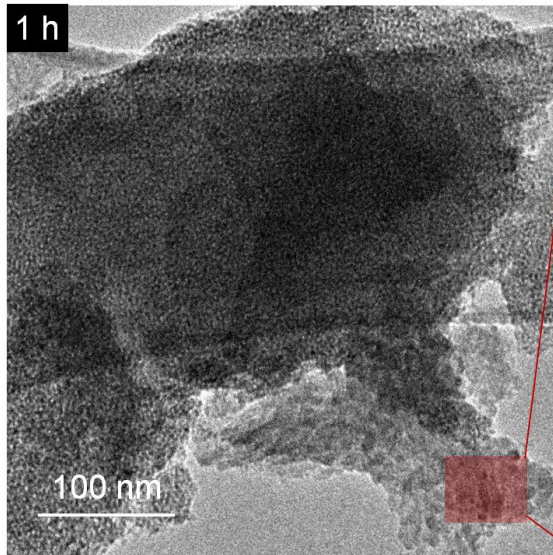
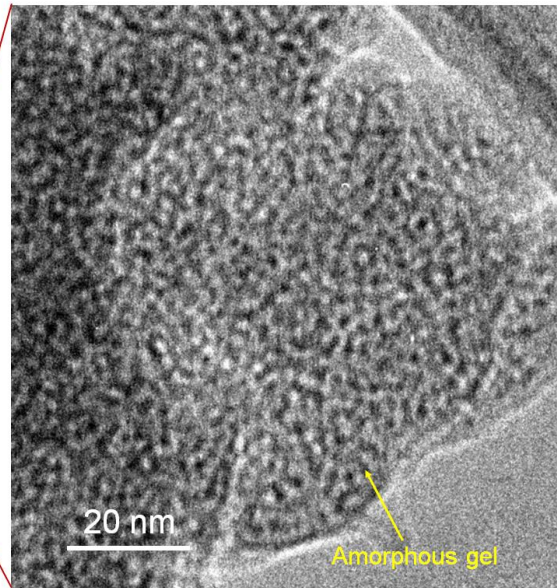
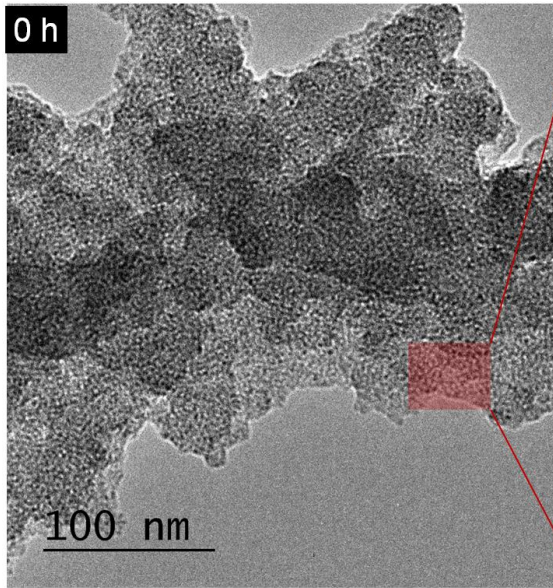
For the synthesis of the titania nanosponge, 0.72 g of PVP was dissolved in 15 ml of anhydrous DMF with magnetic stirring. 1.98 ml of titanium chloride was added to this solution dropwise with the stirring. The solution was refluxed for 1 d to form phenol-Ti-O bonding, completely. Then, 6.48 ml of distilled water was added to this solution. The solution was placed in an oil bath at 373 K for 30 h. The precipitated product was collected by centrifugation and dried in a convection oven at 373 K. The mesopores can be opened by calcination treatment in air at 623 K, which decomposes the polymer. A trace amount of remaining carbonaceous residue in the samples could be completely removed with ozone flow at 573 K.

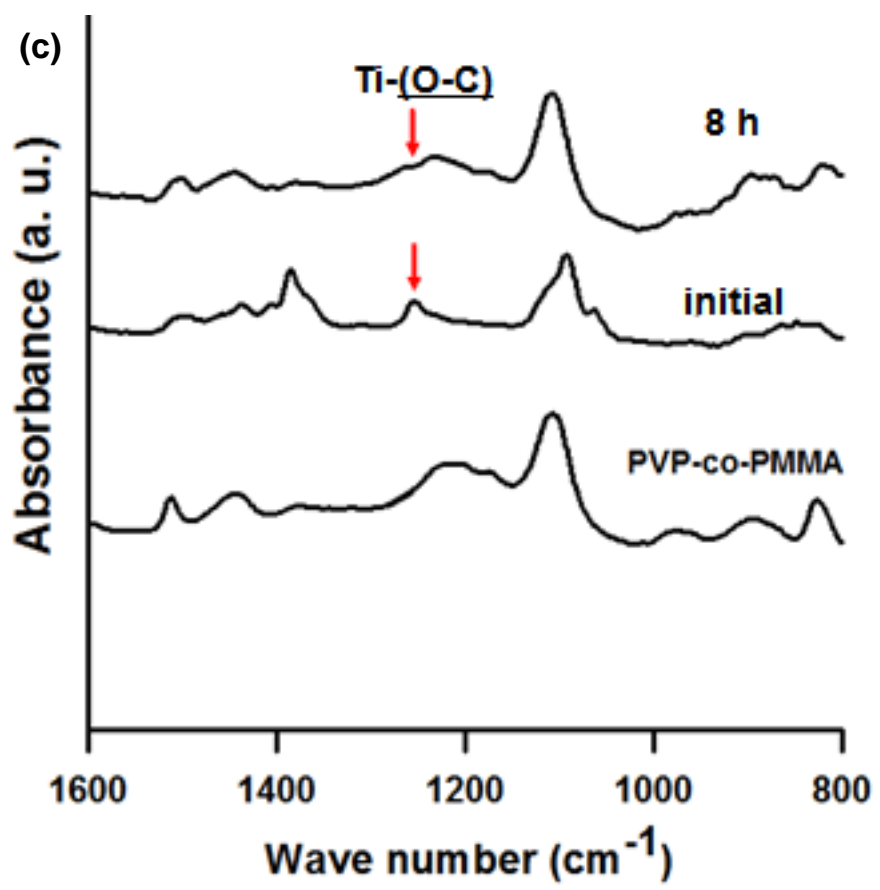
7.2. Mechanistic study of TiO₂ nanosponge formation in random polymer directed synthesis

Solvothermal synthesis of TiO₂ nanosponge was performed for the mechanistic study according to the *Procedure B* described Supporting Information 7.1. During the course of solvothermal treatment, solid precipitates were collected at 0, 0.5, 1, 4 and 8 h. XRD patterns (a) and TEM images (b) of all the solid precipitates are shown below. 0 h sample exhibited a small angle XRD peak at approximately 2.5°, indicating that there was short-range ordering in amorphous inorganic gel-polymer matrix. TEM image of 0 h sample shows mesostructured gel-like feature. These results indicate that mesostructured polymer inorganic composite gels were initially formed. FT-IR spectrum (c) of the mesostructured gel indicates that there were tight Ti-O-C bonding (indicated by red arrow) between phenol groups of polymer and TiCl₄ precursors (*J. Chem. Soc., Dalton Trans.*, **1982**, 271). The tight Ti-O-C bonding led to an increase in inorganic concentration along the polymer chain, which promoted polymerization of inorganic species to form a mesostructured polymer-inorganic composite gel. As the solvothermal treatment was performed, the center of a small angle XRD peak was shifted gradually from 2.5° to 1.2° (see XRD patterns of 4 and 8 h sample). Whereas, wide-angle XRD peaks (25°, 38°, 48°, 55° and 63°) corresponding to anatase TiO₂ appeared. TEM images also show that tiny TiO₂ crystals were generated by the solvothermal treatment. TEM image of 8 h sample shows 4.0 nm of average inter-spacing between tiny crystals. The XRD and TEM results indicate that polymer-inorganic composite gel was transformed to nanosponge-type TiO₂ crystals with anatase frameworks in the course of solvothermal treatment. Meanwhile, tight Ti-O-C bonds between phenol groups of polymer and Ti atoms in titania framework was still retained, as shown in FT-IR spectrum (c). It is particularly note that a well-resolved reflection peak centered at 1.2° was not observed at all in initial stage. Therefore, TiO₂ crystallization might induce the mesostructure formation. In that, when the anatase crystal started to grow from the polymer-inorganic composite gels, the polymer segments are excluded from crystallization, so that polymer backbones become crowded around surfaces of inorganic crystals. Consequently, the polymer segments near the surfaces cause steric hindrance, which limit crystal growth to a scale of only a few nanometers.



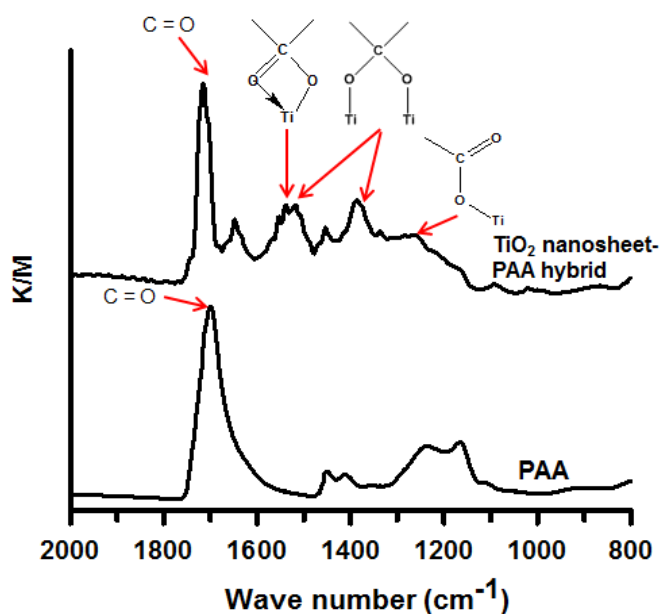
(b)





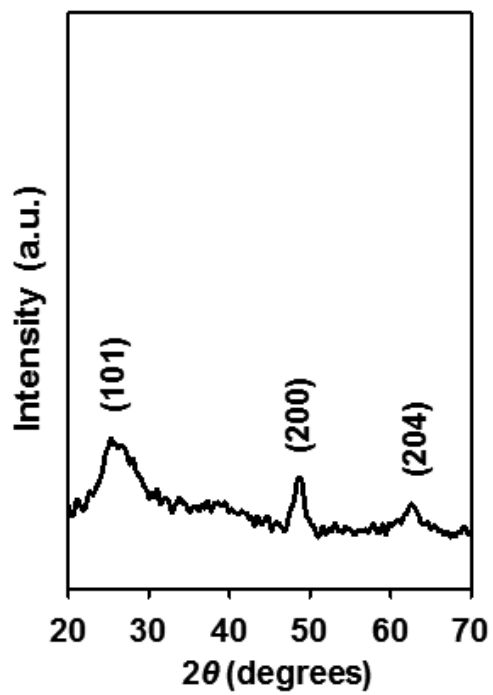
7.3. Solid-state specular reflection FT-IR spectra of the PAA polymer and crystalline TiO₂ nanosheet-PAA hybrid material.

TiO₂ nanosheet-PAA hybrid materials exhibited the characteristic absorption bands of Ti-COO complex bonds, which were indicated by red arrows [*i.e.*, bidentate ligand (1521 and 1458 cm⁻¹), bridging ligand (1560 and 1419 cm⁻¹), and monodentate ligand (1276 cm⁻¹)]. The value of the IR bands was referred to the previous report (*Ceramics International* **2007**, 33, 643, *Journal of Molecular Catalysis A: Chemical* **2012**, 355, 161). This result clearly shows that carboxylate groups of PAA is still strongly bound to TiO₂ nanosheet through coordination bonding after crystallization.

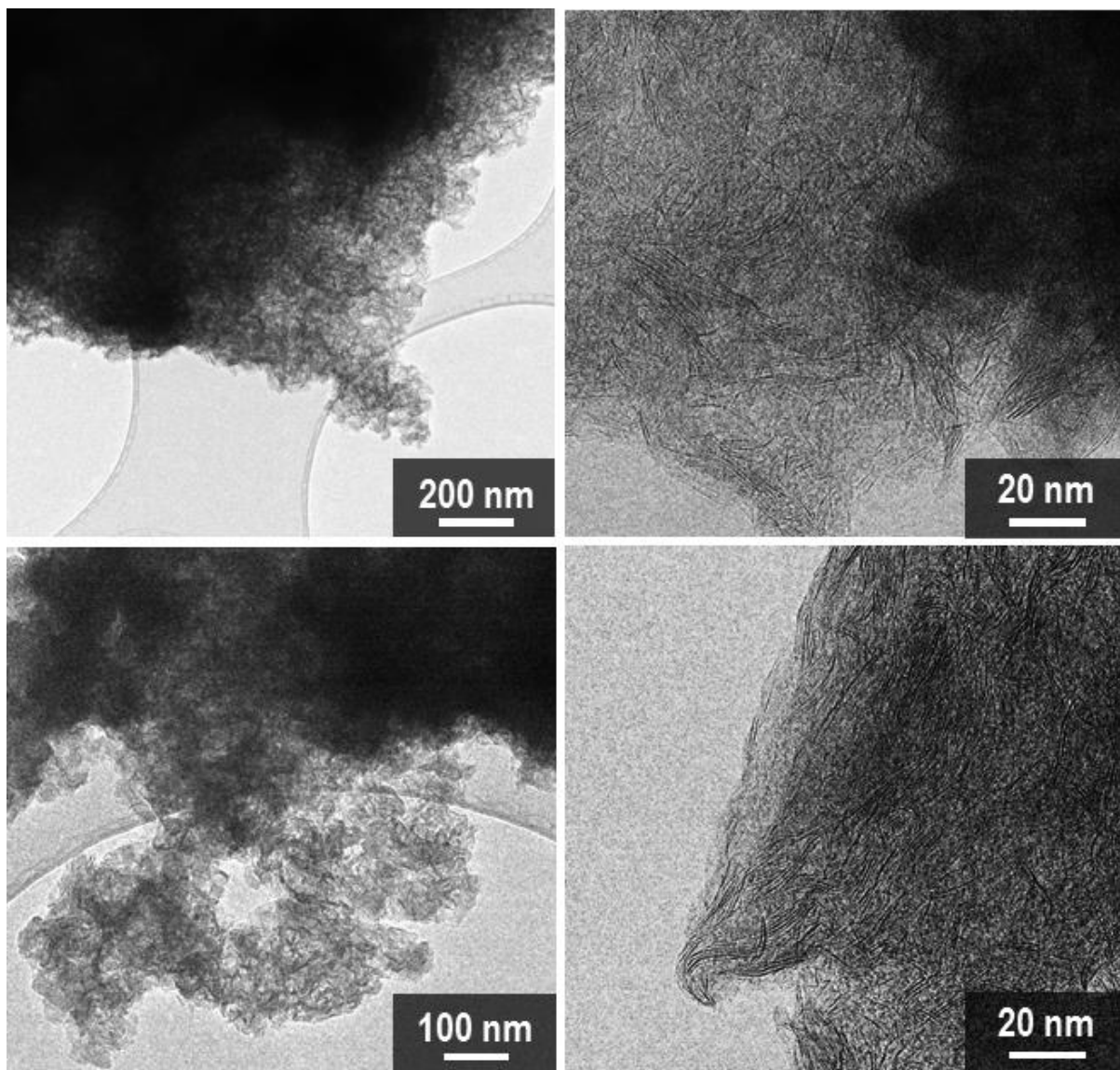


7.4. Characterization results of titania nanosheets

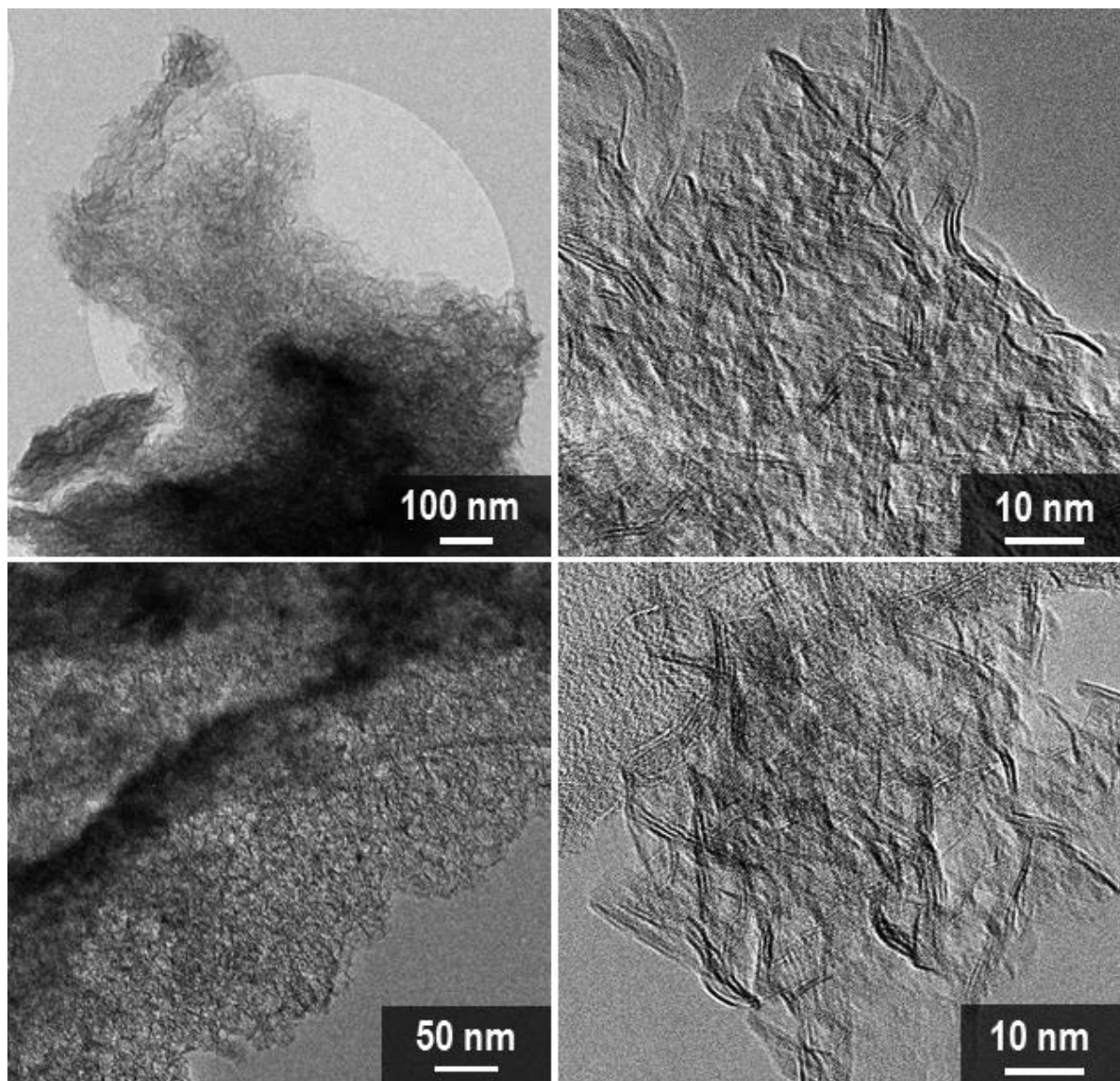
(a) XRD pattern of as-synthesized titania nanosheet



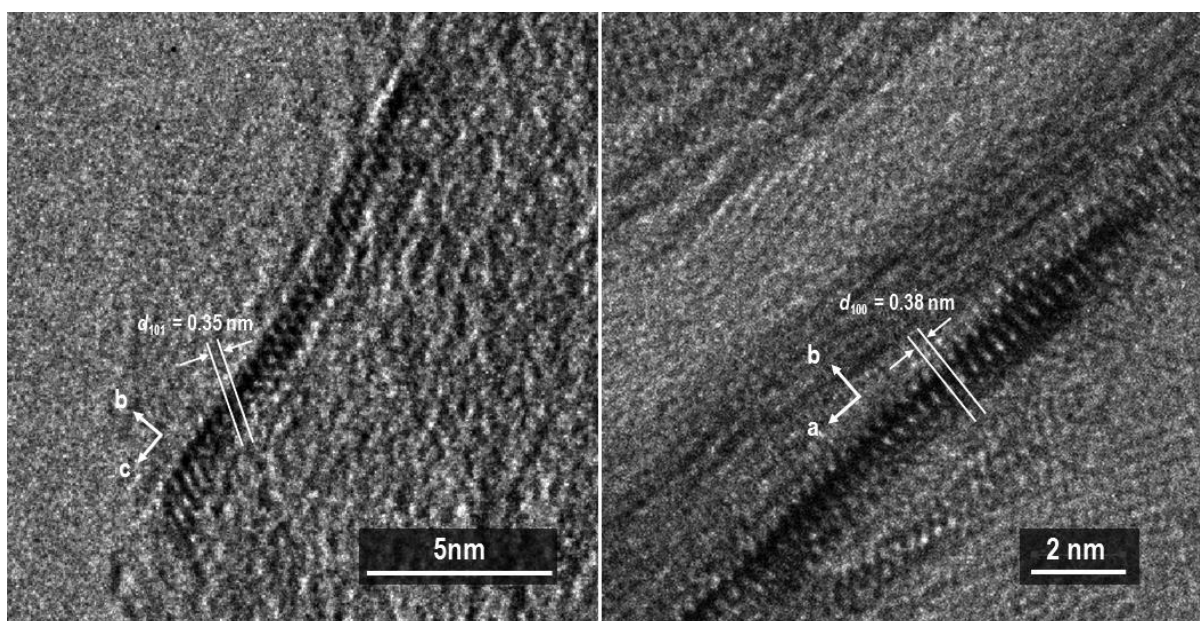
(b) TEM images of the as-synthesized titania nanosheet



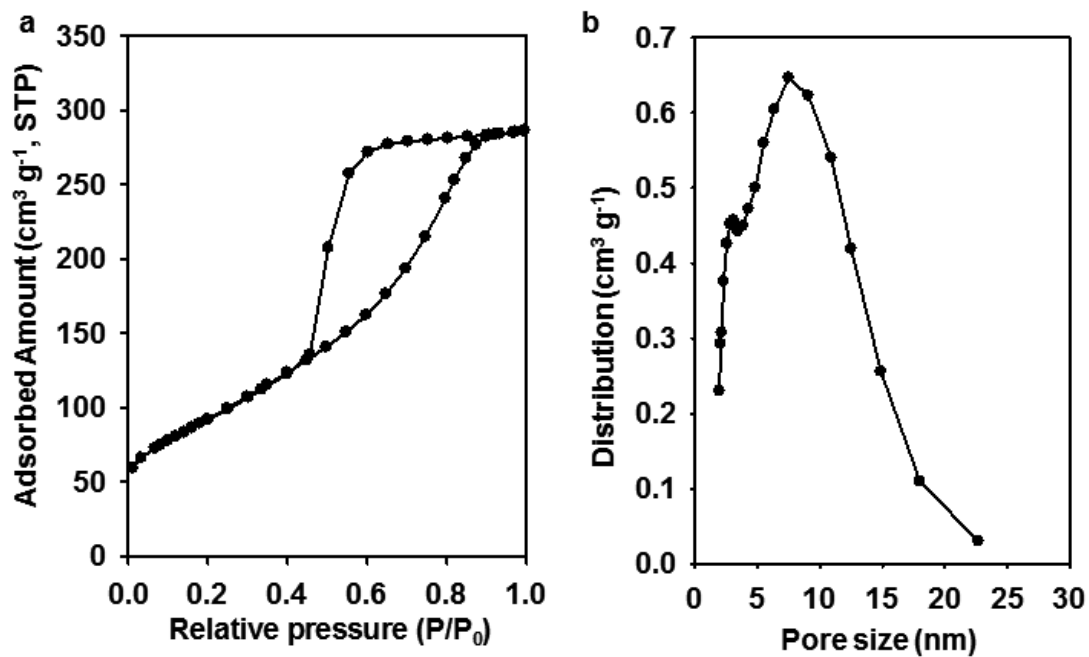
(c) TEM images of the calcined titania nanosheet



(d) HR-TEM images of titania nanosheet taken along two different axes. The HR-TEM images show that titania nanosheets are extremely thin along the *b*-direction.

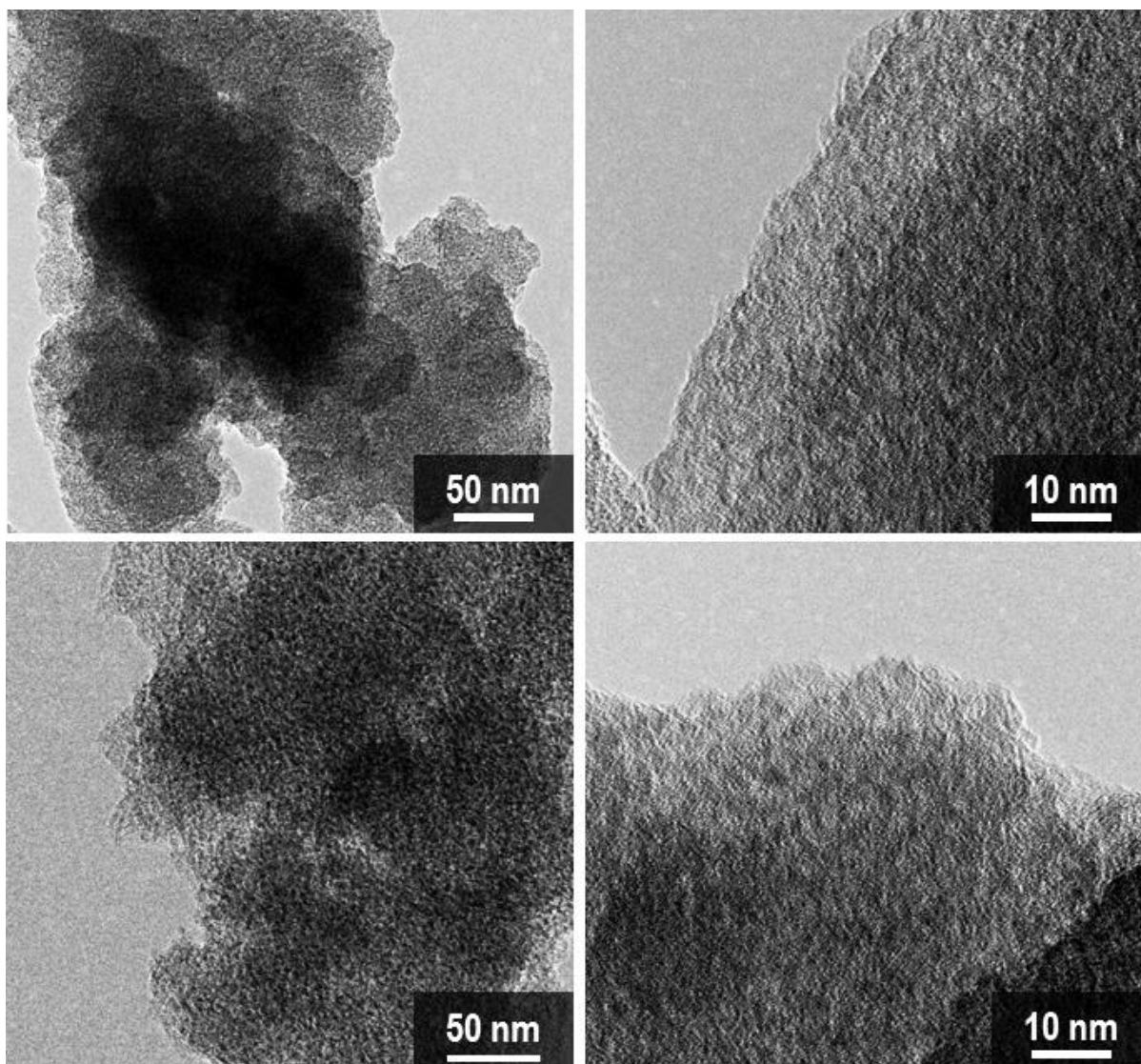


(e) N_2 isotherm of the calcined titania nanosheet and corresponding mesopore-size distribution derived by BJH method.

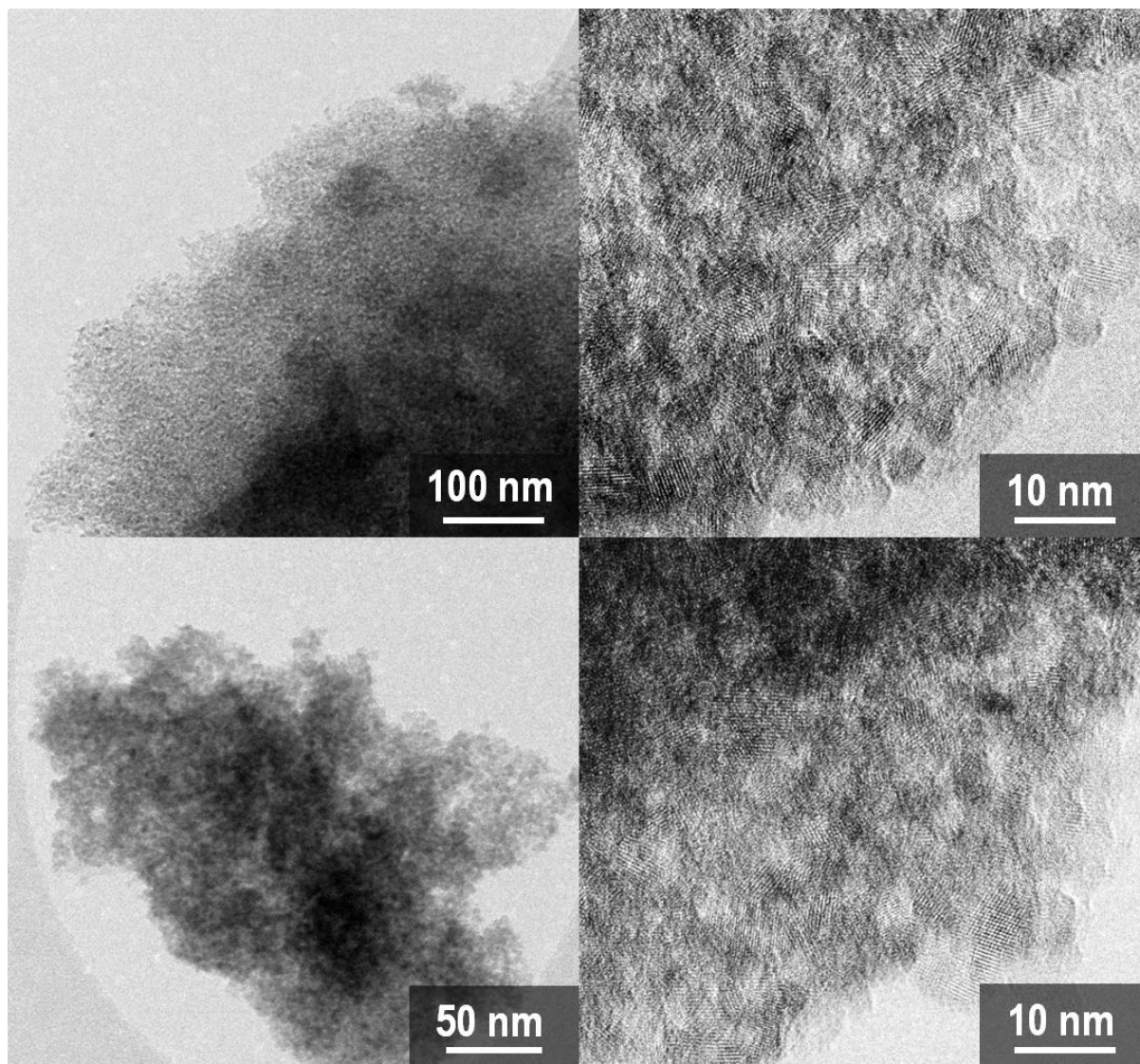


7.5. Characterization results of titania nanosponge

(a) TEM images of the as-synthesized titania nanosponge



(b) TEM images of the calcined titania nanosponge



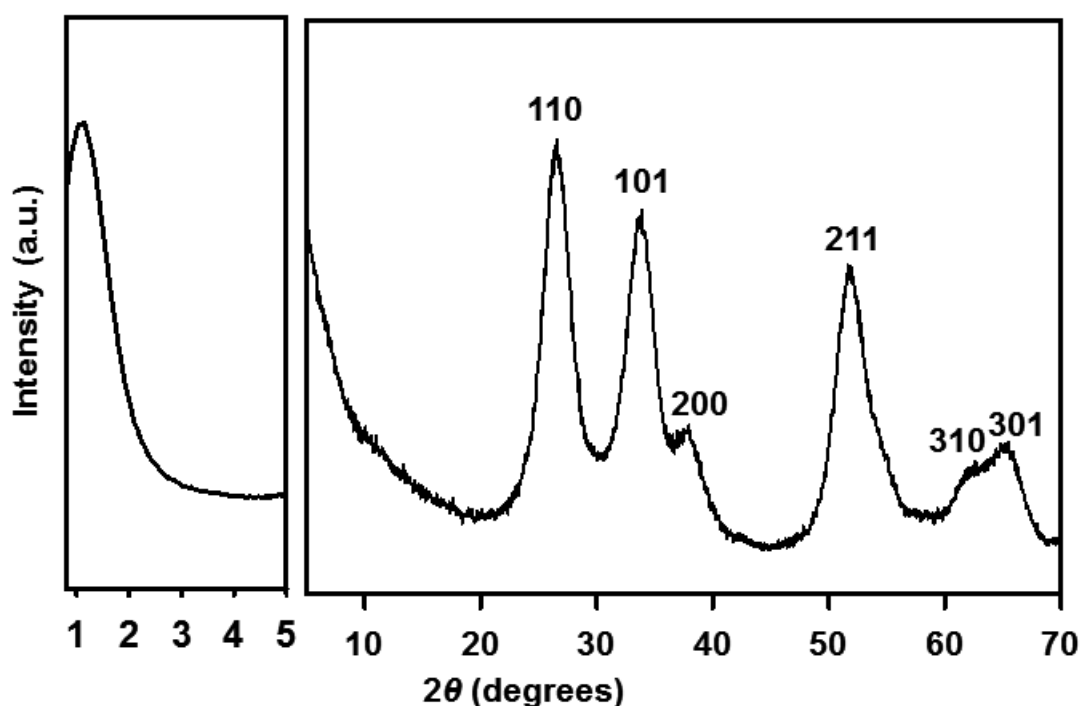
Section S8. ZrO₂ and SnO₂ nanosponges synthesized using a polymer-directed crystallization mechanism

8.1. Preparation of ZrO₂ and SnO₂ nanosponges

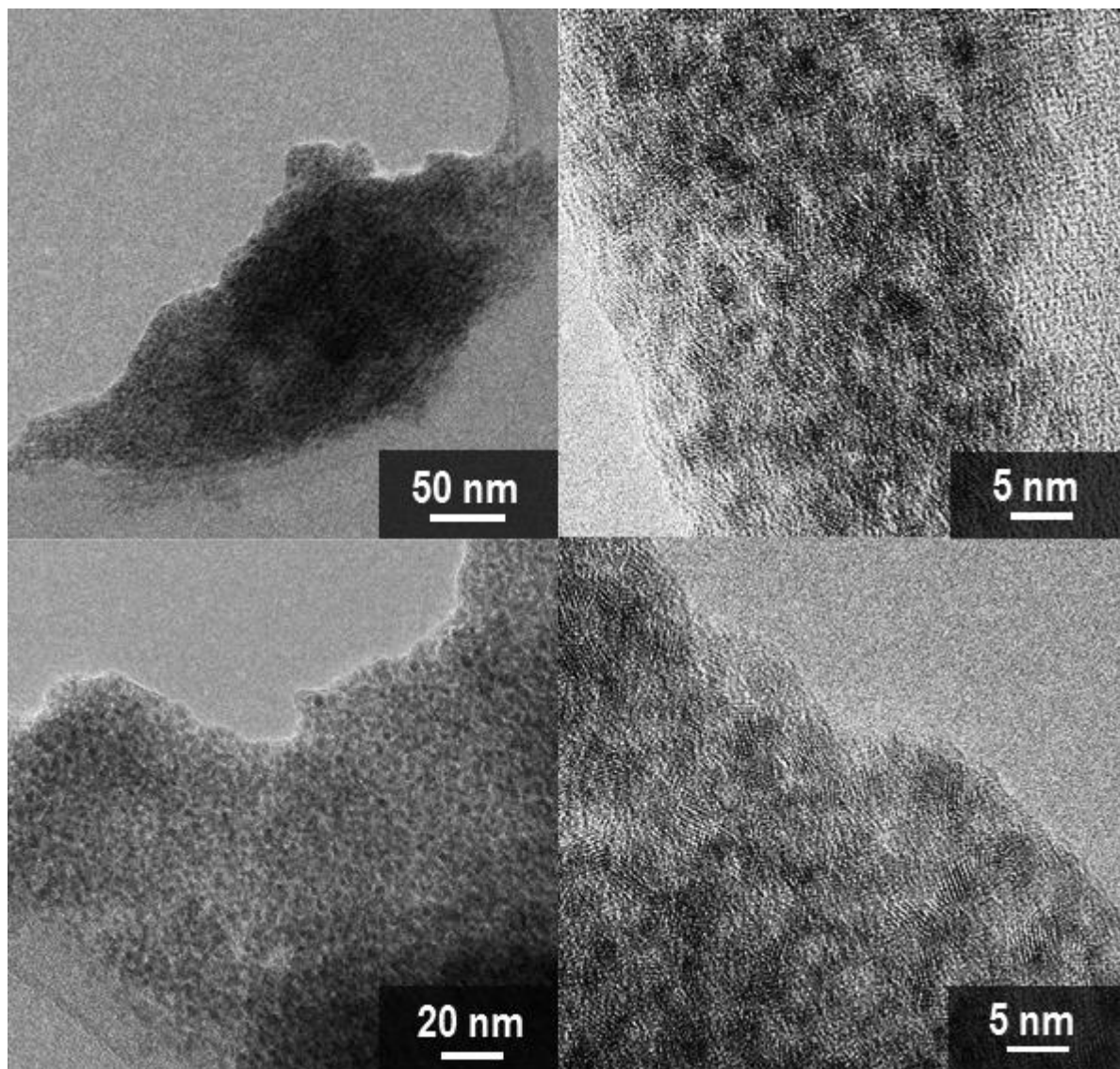
ZrO₂ and SnO₂ nanosponges were solvothermally synthesized using PVP-*co*-PMMA in DMF solution, following *procedure B* in Supporting Information 7.1.(b), except for the use of ZrCl₄ (Aldrich, 99.99%) and SnCl₄ (Aldrich, 99%) as inorganic precursors.

8.2. Characterization results of SnO₂

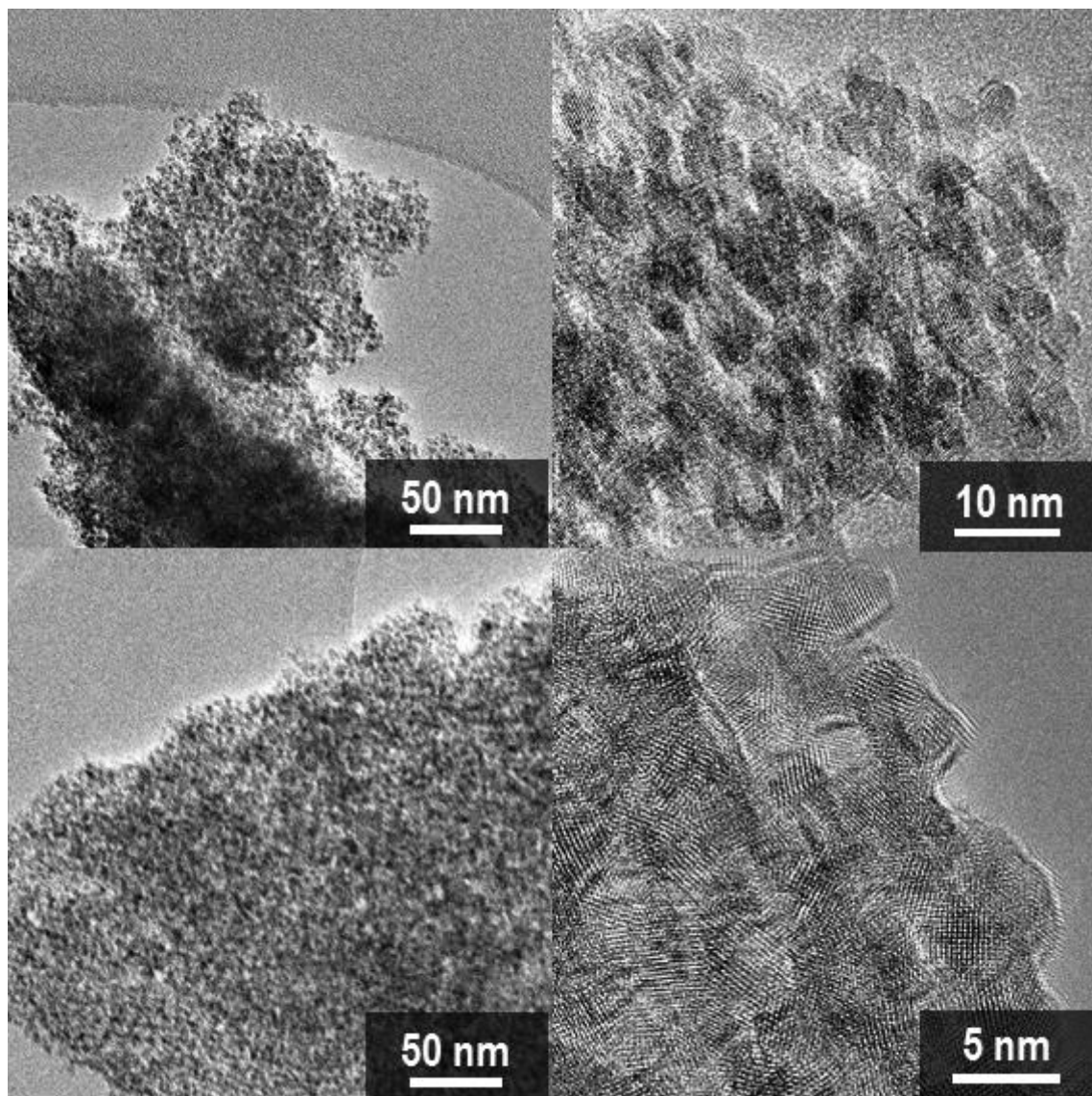
(a) XRD pattern of the as-synthesized SnO₂ nanosponge. A well-resolved low-angle XRD patterns indicated that there should be significant short-range structural ordering in the SnO₂ nanosponge. The XRD pattern exhibited diffraction peaks corresponding to (110), (101), (200), (211), (310), and (301) reflections of typical cassiterite crystal structure of SnO₂.



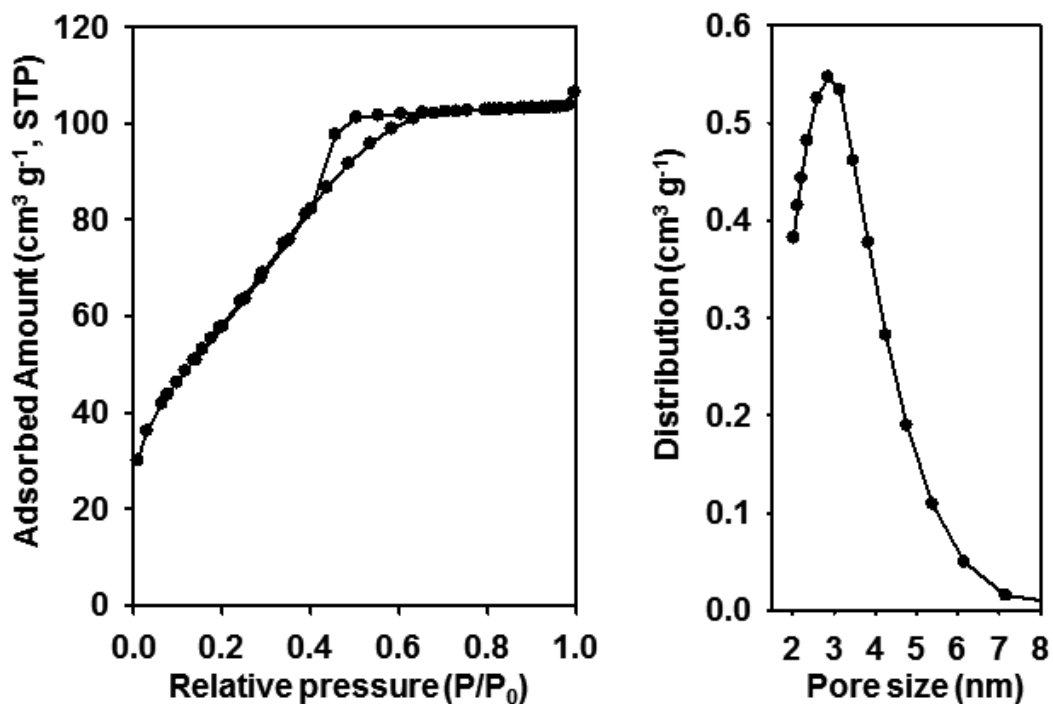
(b) TEM images of the as-synthesized SnO₂ nanosponge.



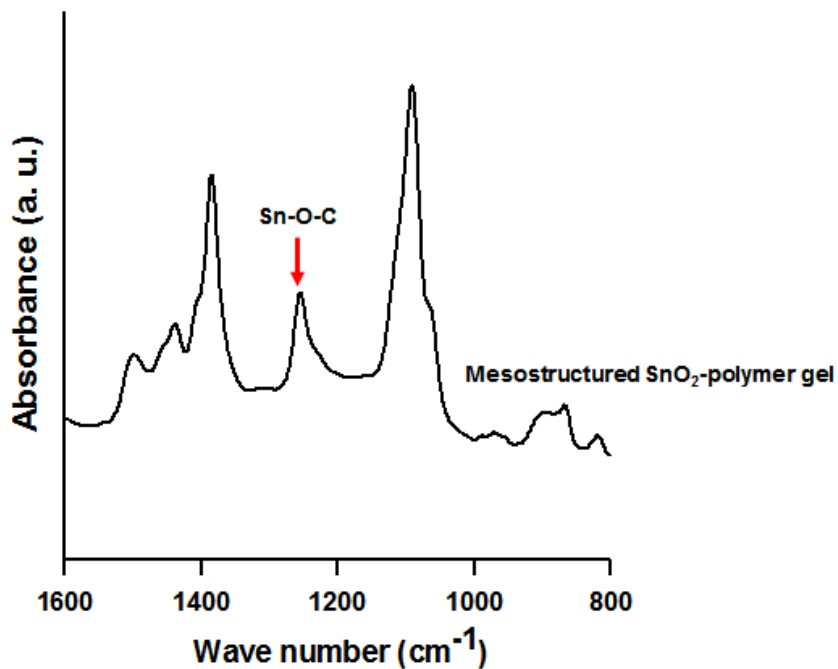
(c) TEM images of the calcined SnO₂ nanosponge.



(d) N_2 isotherm of the calcined SnO_2 nanosponge and corresponding mesopore-size distribution derived by BJH method. The specific surface area of the SnO_2 nanosponge measured by the BET method was $242\text{ m}^2\text{g}^{-1}$. Single-point total pore volume at $P/P_0 = 0.95$ is 0.16 ml g^{-1} .

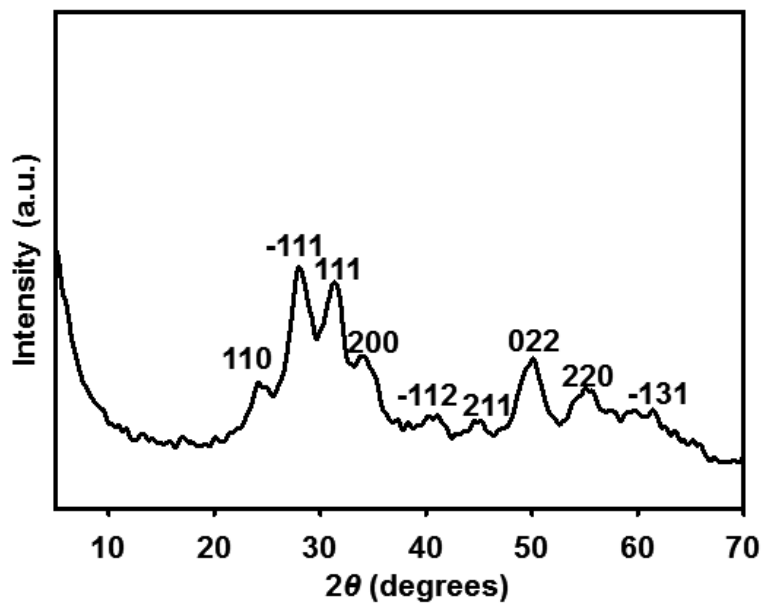


(e) FT-IR spectrum of mesostructured SnO_2 -polymer gel.

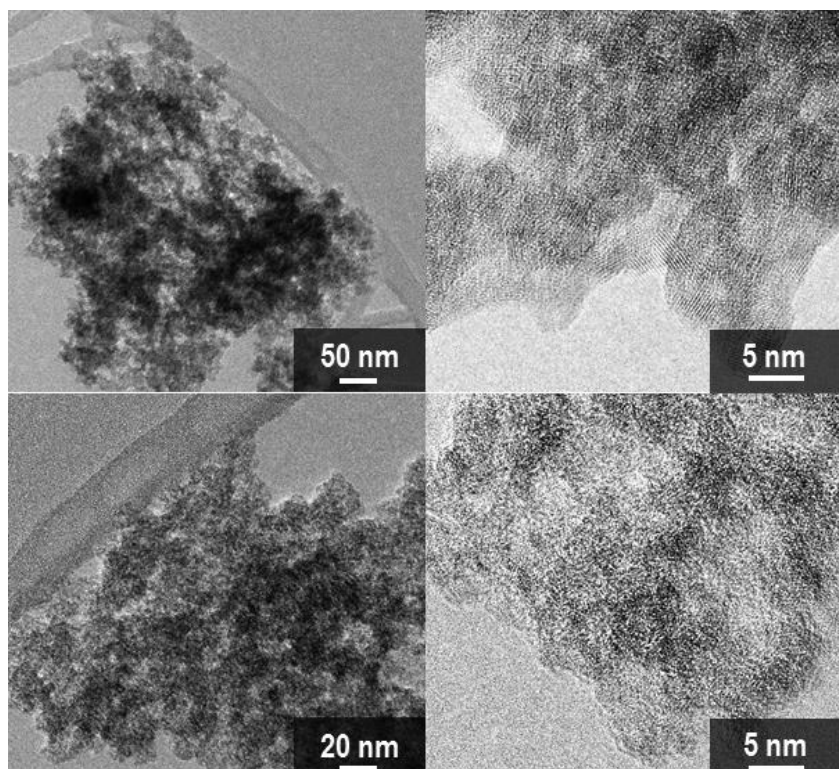


8.3. Structure characterization of ZrO₂

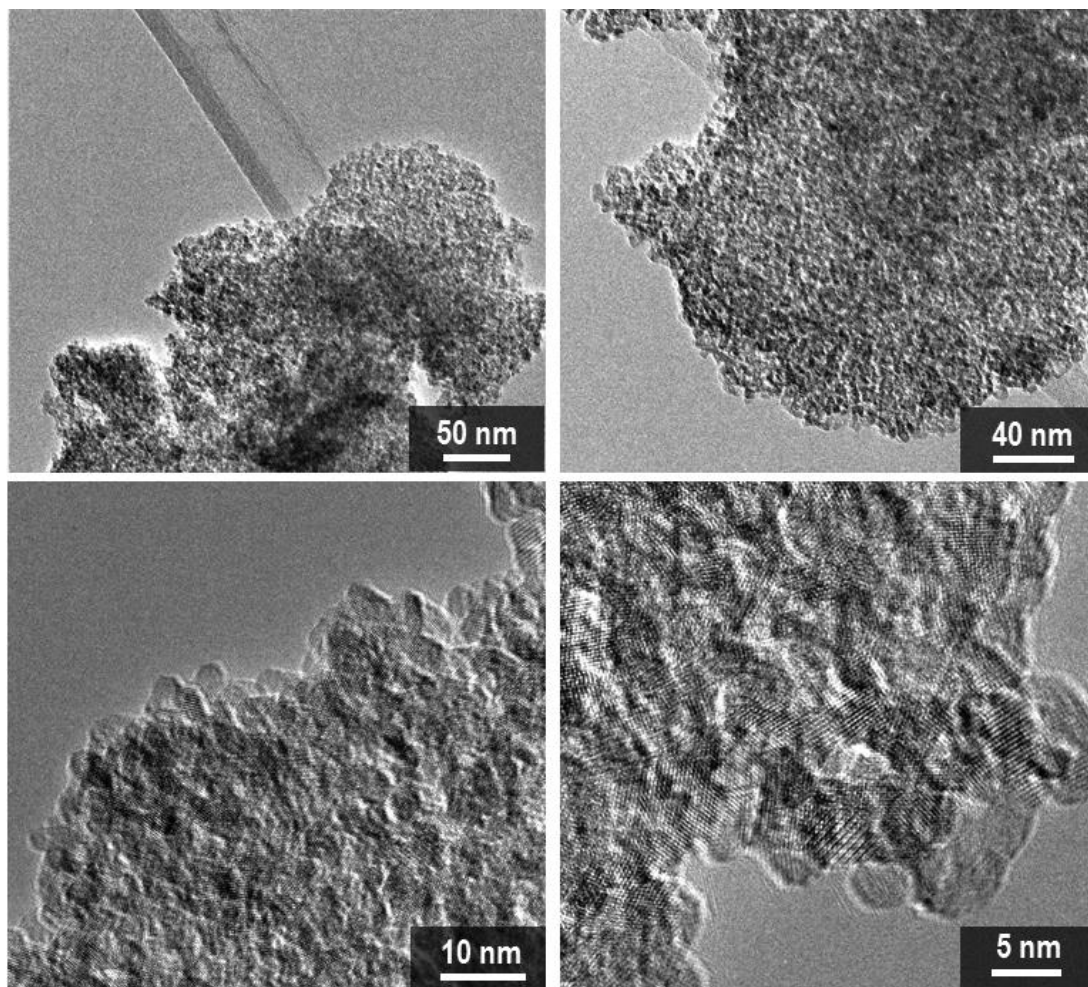
(a) XRD pattern of the as-synthesized ZrO₂ nanosponge. The XRD pattern exhibited diffraction peaks corresponding to typical monoclinic crystal structure of ZrO₂.



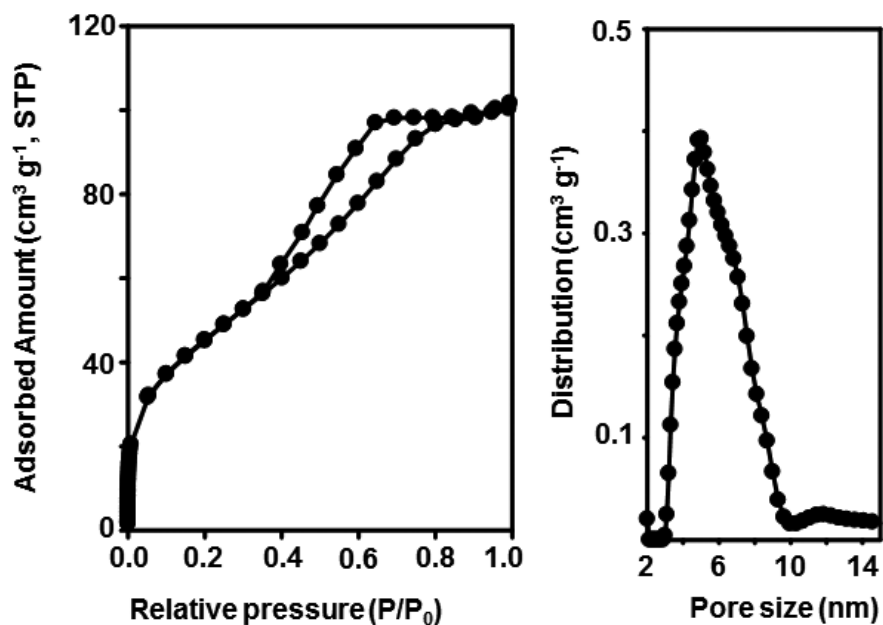
(b) TEM images of the as-synthesized ZrO₂ nanosponge.



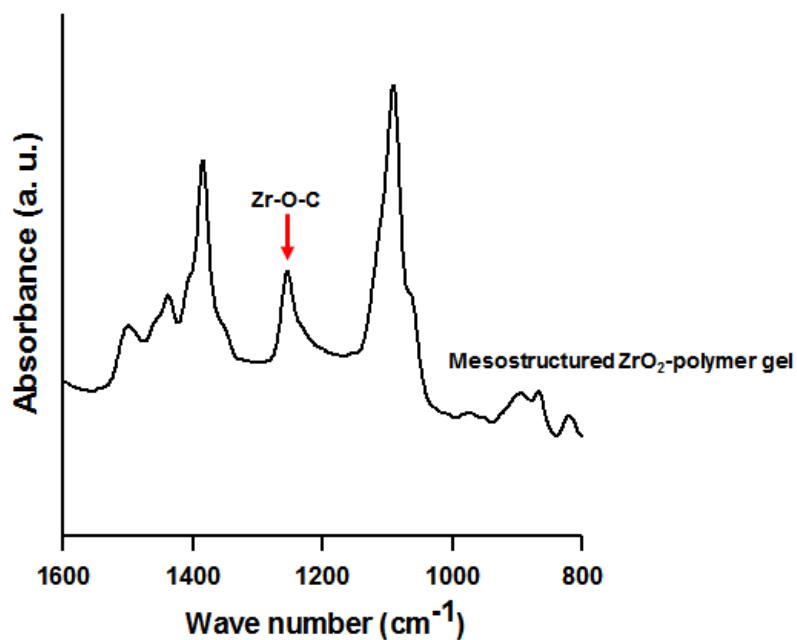
(c) TEM images of the calcined ZrO_2 nanosponge.



(d) N_2 isotherm of the calcined ZrO_2 nanosponge and corresponding mesopore-size distribution derived by BJH method. The specific surface area of the ZrO_2 nanosponge measured by the BET method was $142\text{ m}^2\text{g}^{-1}$. Single-point total pore volume at $P/P_0 = 0.95$ is 0.15 ml g^{-1} .



(e) FT-IR spectrum of mesostructured ZrO_2 -polymer gel.



Characterization methods

High-resolution synchrotron X-ray powder diffraction data of MFI zeolite and TiO₂ were measured at 9B beamline at PLS-II. The incident X-rays were vertically collimated by a mirror, and monochromatized to the wavelength of 1.5463(1) Å using a double-crystal Si(111) monochromator. The detector arm of the vertical scan diffractometer is composed of soller slits, flat Ge(111) crystal analyzer, anti-scatter baffle, and scintillation detector. XRD patterns of the beta zeolite, phosphates and SnO₂ (and ZrO₂) nanosponges were obtained at KAIST using a Rigaku Multiflex diffractometer using a monochromatized X-ray beam from Cu K_α radiation (40 kV, 30 mA). Transmission electron microscopy (TEM) images were obtained with a TitanTM ETEM G² at 300 kV at room temperature. Scanning electron microscopy (SEM) images were obtained with a Hitachi S-4800 at a low landing energy (3.0 kV, in a gentle-beam mode) and Magellan400 at a low landing energy (1.0 kV), without metal coating. Argon adsorption-desorption isotherms were measured at liquid argon temperature (87 K) with a Micromeritics ASAP2020 volumetric adsorption analyzer. Nitrogen adsorption-desorption isotherms were measured at 77 K using a Micromeritics TriStar II volumetric adsorption analyzer. The Brunauer–Emmett–Teller equation was used to calculate the apparent surface area from the adsorption data obtained at P/P_0 between 0.1 and 0.3. Pore size distributions for hierarchical zeolites and TiO₂ nanosponge were calculated from argon adsorption isotherms using nonlocal density–functional–theory NLDFT methods. Pore size distributions for aluminophosphate and SnO₂ (and ZrO₂) were calculated from N₂ adsorption isotherms using Barrett-Joyner-Halenda methods.

¹H NMR (Bruker Avance instrument 300 MHz) was used to identify the organic molecules synthesized here. Two-dimensional (2D) NMR experiments for aluminophosphate were performed using a Bruker AVANCE III 400 MHz NMR spectrometer with an 9.4 Tesla superconducting magnet. A Bruker 1H/X double–resonance MAS probehead with 4–mm zirconia rotors was used under conditions of MAS at 9 kHz. ³¹P NMR spectra were acquired with simultaneous proton decoupling by applying the Small Phase Incremental Alternation using 64 steps (SPINAL–64) pulse sequence with a 1H rf field of 100 kHz. ³¹P{¹H}cross–polarization measurements were conducted adiabatically using a contact time of 2.0 ms. The HETCOR NMR technique is a 2D extension of the 1D CP–MAS NMR experiment, providing enhanced spectral resolution. Double Fourier transformation converts the time domain signal S (t1, t2) into the frequency domain S (ω1, ω2), which is presented here as a 2D contour plot spectrum to 15% of full signal intensity. Hypercomplex time–proportional–phase–incrementation (STATES–TPPI) quadrature detection was used for the indirect dimension. ³¹P chemical shifts were referenced to aluminophosphate-14 (AlPO₄-14) with tetramethylsilane (TMS, Si(CH₃)₄) as a ³¹P and ¹H secondary chemical shift reference.

²⁹Si NMR spectra for zeolite samples were acquired using a Bruker AVANCE400WB spectrometer with 7 mm probehead at room temperature. The ²⁹Si MAS NMR spectrum was taken in a single-pulse sequence with a pulse width of 7.6 μs, a relaxation time of 60 s and a spinning frequency of 5 kHz. ²⁹Si chemical shifts were referenced to 4,4-dimethyl-4-silapentane-1-sulfonic acid.